Relative Efficiency of Surface Energy Budgets Over

Different Land Covers

by

Jiachuan Yang

A Thesis Presented in Partial Fulfillment
of the Requirements for the Degree
Master of Science

Approved November 2012 by the
Graduate Supervisory Committee:

Zhihua Wang (Chair)
Enrique Vivoni
Larry Mays
Huei-Ping Huang

ARIZONA STATE UNIVERSITY

December 2012

ABSTRACT

The partitioning of available solar energy into different fluxes at the Earth's surface is important in determining different physical processes, such as turbulent transport, subsurface hydrology, land-atmospheric interactions, etc. Direct measurements of these turbulent fluxes were carried out using eddy-covariance (EC) towers. However, the distribution of EC towers is sparse due to relatively high cost and practical difficulties in logistics and deployment. As a result, data is temporally and spatially limited and is inadequate to be used for researches at large scales, such as regional and global climate modeling. Besides field measurements, an alternative way is to estimate turbulent fluxes based on the intrinsic relations between surface energy budget components, largely through thermodynamic equilibrium. These relations, referred as relative efficiency, have been included in several models to estimate the magnitude of turbulent fluxes in surface energy budgets such as latent heat and sensible heat. In this study, three theoretical models based on the lumped heat transfer model, the linear stability analysis and the maximum entropy principle respectively, were investigated. Model predictions of relative efficiencies were compared with turbulent flux data over different land covers, viz. lake, grassland and suburban surfaces. Similar results were observed over lake and suburban surface but significant deviation is found over vegetation surface. The relative efficiency of outgoing longwave radiation is found to be orders of magnitude deviated from theoretic predictions. Meanwhile, results show that energy partitioning process is influenced by the surface water availability to a great extent. The study provides

insight into what property is determining energy partitioning process over

different land covers and gives suggestion for future models.

ACKNOWLEDGMENTS

First of all, I would like to thank my committee members Professor Zhihua Wang, Professor Larry Mays, Professor Huei-ping Huang and Professor Enrique Vivoni, for supervising and guiding my research work. Their invaluable opinions greatly enlighten my research experience.

This work would not have been accomplished without the field measurements from several research groups. Here I would like to express my thanks to Professor Marc Parlange and the rest of the Environmental Fluid Mechanics and Hydrology Laboratory at the Swiss Federal Institute of Technology—Lausanne for sharing the lake dataset; to Professor Elie Bou-Zeid and the rest of the Environmental Fluid Mechanics Group at Princeton University for sharing the suburban EC dataset; and to Professor James Smith, Dr. Mary-Lynn Baeck and the rest of the Hydrometeorology Research Group at Princeton University for sharing the grass field dataset.

Finally, I would like to express special thanks to my family, my friends and my schoolmates, especially to my girlfriend Yongshi Zhao. They have encouraged me a lot and shared my happiness in daily life. Their support is really important for my work.

TABLE OF CONTENTS

LIST OF FIGURES

LIST OF FIGURES

Chapter 1

INTRODUTION

1.1 Background

Among all sustainable energies, solar radiation is the most constant source
for the earth. After travelling through several atmospheric layers, the radiation
arrives at the Earth's surface and partitions into turbulent and ground heat fluxes.
Only the lower part of the atmosphere, i.e. the atmospheric boundary layer (ABL),
will be directly affected by the heat fluxes, which responds to surface forcing with
a timescale of about an hour or less. Over the ABL is the "free atmosphere" where
the wind is nearly geostrophic and turbulence is only intermittent. Climate change
and weather variations occur mainly within this near-surface layer, which attracts
a tremendous amount of recent research effort. A thin layer at the bottom, roughly
10%, of the ABL is of particular interest to researchers because it is where human
activities concentrates and response to the surface irradiance immediately occurs.
This thin layer, named as the atmospheric surface layer (ASL), is the focus area of
this study.

Figure 1.1 shows the schematic of surface energy budget. In the view of
energy partitioning, near-surface energy balance can be written as:

$$\frac{dS}{dt} = d(R_n - H - LE - G)/dz \qquad (1.1)$$

where S is the energy storage within the system, t is the time, R_n is the net
radiation, H is the sensible heat flux, LE is the latent heat flux and G is the ground

heat flux. If the study domain is selected to be infinitesimally thin, the storage

term *S* within the domain is negligible, equation (1.1) can be rewritten as:

$$R_n = H + LE + G \qquad (1.2)$$
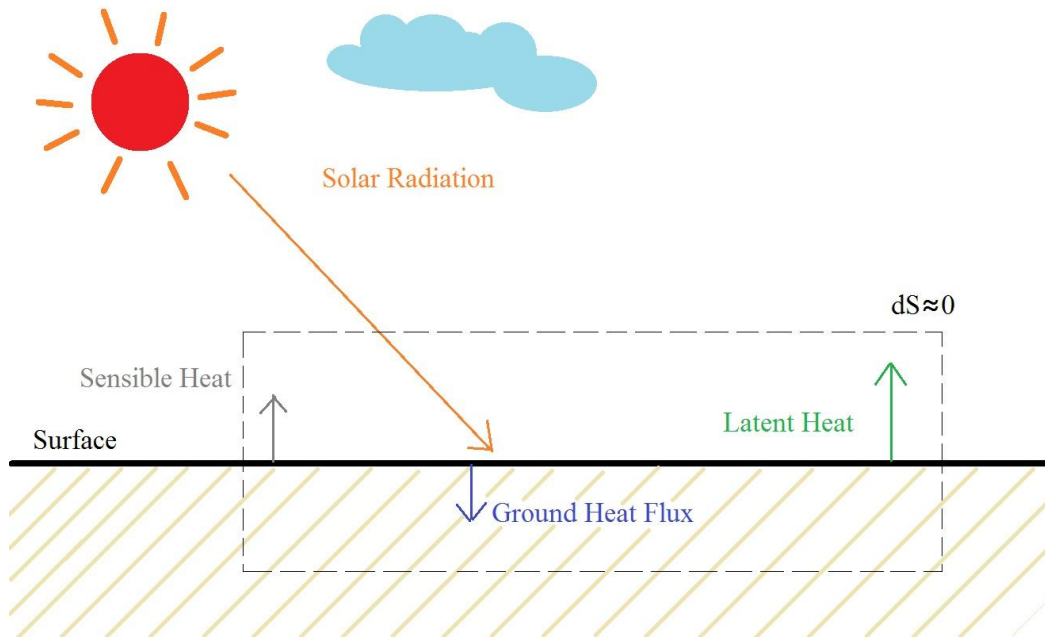
Figure 1.1. Schematic of surface energy budget

From equation (1.2), it is shown that solar radiation is actually partitioning

into three dissipative fluxes near surface, which have their own importances in

different processes. The magnitude of *G* has a direct and significant influence on

soil temperature and will affect the rate of underground biochemical processes.

The magnitude of *LE* is directly related to the hydrological cycle through the

evaporation rate, which affects processes such as cloud forming and moisture

exchange significantly. The magnitude of *H* will affect the evolution of surface

heating and drying, influence the structure of air temperature in the boundary

layer and act to force the dynamics and thermodynamics of the low troposphere.

Thus the efficiency of dissipating the solar energy into these three fluxes is

important in determining dynamic and thermodynamic properties of both the ABL and soil layers beneath earth surface.

The first period when turbulent fluxes were of great interest to researchers were in the 1940s, whereas high frequency measurements commonly used today is not available. During the period, turbulent fluxes were determined by flux-profile relations through the gradient of mean variables with respect to altitude, such as gradient of wind speed, specific humidity and air temperature. Measurements from different heights were compared and conclusions were drawn mainly on the scale as well as on the trend of turbulent fluxes with respect to height (Cramer and Record 1953; Swinbank 1955; Deacon 1955). One important finding as a general principle is that turbulent fluxes are effectively constant with height from the top of the layer where molecular effects are significant, up to a height of several meters and even to 100 meters around noon under insolation.

After high frequency measurements are available, these turbulent fluxes, as dissipative components of surface energy balance (SEB), have been routinely observed at selected point locations where instruments were installed on tower platforms. However, those networks of tower sites are with limited spatial distribution because of their relatively high cost. Thus it is impossible to coverage and map fluxes such as *H* or *LE* based on tower observations alone. Besides the spatial limitation, another problem that may exist at the tower site is that not all flux terms in SEB are measured. This may be due to the different interest of the researchers, the limitation of the funding or the specific site condition. For example, ground heat flux is usually not measured in urban areas because it is

difficult to insert sensors into pavements. The inconsistent setup and measurement

standard further increase the limitation of EC datasets. On the other hand, for

mapping at a relatively large scale, the remote sensing technique has the

advantage of wide spatial coverage. However, they are not able to sense the fluxes

directly and empirical relations are needed.

In addition, there are many approaches using land surface temperature

(LST), vegetation indices (VI) and soil moisture or other directly sensed variables

to estimate the turbulent fluxes. They may be broadly categorized into three

groups. For the first group, a couple of empirical relations were formed to

estimate the turbulent fluxes based on LST and VI data (Moran et al. 1994;

Sandholt et al. 2002; Kalma et al. 2008). However, these empirical relations

needed turbulent fluxes observation to calibrate the parameters and were still

limited by the data availability. The second group mostly used instantaneous

observations of LST combined with surface high frequency air micrometeorology

measurements to solve the surface energy balance and predict surface heat fluxes

(Anderson et al. 1997; Mecikalski et al. 1999; Jiang and Islan 2001; Kalma et al.

2008). The flux retrieval models developed by this group were diagnostic and

usually required closure assumption, such as the ground heat flux is a given

empirical fraction of the net radiation. And the net radiation was estimated by the

balance between incoming and outgoing longwave and shortwave radiation. The

third group tried to infer LE and H from the remote sensing data based on that the

evolution of LST implicitly contained information about the history of energy

partitioning among the SEB components. LST measurements were input into the

force-store equation to estimate the evaporative fraction ($LE/(LE+H)$) and bulk

heat transfer coefficient (Crow and Kustas 2005; Sini et al. 2008), then the

turbulent fluxes were computed based on these parameters. This approach was

built on the assumption that the ratio of latent heat to sensible heat is constant

during daytime in cloudy-free conditions with intense solar radiation forcing

(Gentine et al. 2007, 2011).

Besides using the directly sensed variables with developed equations to

estimate the fluxes, a way to estimate fluxes from thermodynamic principles, in

particular, the entropy production rate, was recognized and developed. The

well-known second law of thermodynamics dictates that, the entropy of a closed

system is always increasing. Entropy production is then defined as the change rate

of the entropy of the closed system. Lorenz (1960) hypothesized that the Earth's

atmosphere operates in a manner that generates available potential energy at a

possible maximum rate. Independently, Paltridge (1975) suggested that the mean

state of the present climate is reproducible as a state with a maximum rate of

entropy production without considering the detailed dynamics of the system. His

prediction was shown to be in remarkable agreement with observations, and the

same result was obtained by several other researchers later (Mobbs 1982; Ozawa

and Ohmura 1997; Pujol and Llebot 1999).

The maximum entropy production (MEP) theory has been applied to

various kinds of turbulent fluid systems by researchers and shows good

performance. Minobe et al. (2000) carried out numerical experiments of thermal

convection in a rotating fluid system and found the kink at a boundary between

two different convection regimes results from the regime with a higher rate of
entropy production. Shimokawa and Ozawa (2002) carried out numerical
simulations of oceanic general circulation and found that irreversible change
always occurs in the direction of increasing entropy production. These
simulations were all based on the thermodynamic entropy. Jaynes (1957)
developed information theory to assign probability distribution in statistical
mechanics and defined the entropy as a quantitative measurement of information
for any systems that needs to be described probabilistically for making statistical
inferences (Shannon 1948). Dewar (2003, 2005) included the fluctuation theorem
and maximum entropy production (MEP) in the nonequilibrium thermodynamics
and developed novel approaches to model surface fluxes in the nonequilibrium
thermodynamics. He showed that the most probable steady state in macroscopic
scale is the one with MEP among all other possible states, given the boundary
conditions and the conservation equations. This approach bridges the gap between
information entropy and the thermodynamic entropy. The entropy in the MEP
theory is suggested to be not necessarily related to the thermodynamic entropy.

  The methods above focus on estimating turbulent fluxes directly from
field measurements. As discussed above, this approach may not always be
feasible due to data limitation or inconsistent measurements. In this case, an
alternative way to estimate turbulent fluxes is found by using the intrinsic
relations between flux terms in the SEB, which is referred as the relative
efficiency. In this study, relative efficiency of a heat flux is defined as the ratio of
the flux to the sensible heat flux. With the relative efficiency, one can obtain all

the turbulent fluxes in SEB based on a single turbulent flux *H*. And this approach is much faster than estimating the fluxes from EC datasets by imbedding physical processes of surface energy partitioning in the formulation of relative efficiency coefficients. In addition, since turbulent fluxes origin from the net radiation at the surface, the relative efficiency should be modulated by land cover types to a great extent. Thus a same relative efficiency can be applied to different areas as long as the land cover types are similar.

The merits of relative efficiency have already been noticed by many researchers. The most well known relative efficiency, Bowen ratio defined by Bowen (1926), is the ratio of sensible heat to latent heat. After that, Priestly (1959) developed relative efficiency between ground heat flux and sensible heat, sensible heat and latent heat near surface. Based on some assumptions, he simplified the relative efficiency near surface to functions dependent only on surface temperature and the properties of the contacting media. This method works reasonably well in practice over saturated surface. More recently, Wang and Bras (2009, 2011) developed relative efficiencies based on MEP theory with respect to Shannon's entropy, result indicates that model performances well over bare soil and canopy conditions. Bateni and Entekhabi (2012) developed linear stability analysis to quantify the relative efficiency of SEB components. During the analysis LST perturbations to the stable state are converted into a linear form of the dynamic equations, result shows good agreement with two field experiment datasets.

1.2 Problem statement and contribution

In this study, the classical method (Priestley 1959), the MEP theory (Wang and Bras 2009, 2011) and the linear stability analysis (Bateni and Entekhabi 2012) were selected to represent the family of methods using the concept of relative efficiency. All their predictions show good agreement with selected field measurements. However, no research effort has been carried out for an intercomparison among these methods. The first contribution of this study is carrying out the intercomparison among the family of methods to provide great insight into the different mechanisms of models and to give suggestions for future model developments.

Besides, proposed models are using universal approaches that can be applied to different land covers but they have not been consistently verified using a variety of field datasets. The second contribution of this study is collecting datasets and comparing the model performances over various land covers. This comparison gives instructions for model applications over different land covers and helps to find out the potential improvements for existing models.

Among the models, MEP theory is predicting results over surface with different water availability conditions. However, the relation between model results and surface water availability is not explicit. The last contribution of this study is incorporating a scale parameter into the MEP theory to relate the model results to surface water availability more clearly. Incorporating the parameter also facilitates the comparison between results from the LSA model and the MEP model.

1.3 Organization

This thesis, which aims to carry out intercomparison between existing models, is organized as follows. Chapter 2 presents the description of three different methods used in this study, respectively linear stability analysis model by Bateni and Entekhabi (2012), MEP theory model by Wang and Bras (2009, 2011), and classical method by Priestley (1959). Chapter 3 describes the underway experiment over frequently used urban land covers. Chapter 4 contains the information of datasets used in the study and necessary data processing before estimating dissipative fluxes. In chapter 5, model predictions over different land covers are verified using a variety of field datasets. Finally the findings of this study and developments of future models are discussed in chapter 6.

Chapter 2

METHODOLOGY

2.1 Classical method

The classical method in this study was developed by Priestley in 1959. In the model, heat conduction process between air and soil is considered as the process of air mass invading. When an air mass comes into contact with an underlying surface with which it is not in thermal adjustment, the heat will be transferred from one medium to the other at the rate governed by the temperature difference and the wind speed. A schematic of this model is shown in Figure 2.1.
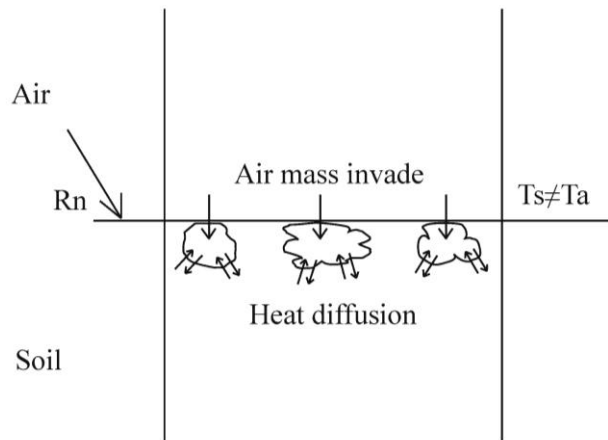

Figure 2.1. Schematic of Priestley model

When surface conditions are sufficiently near to horizontal homogeneity, the governing equation of vertical diffusion in air is generally given as:

$$\frac{\partial T_a}{\partial t} = \frac{\partial}{\partial z}[\kappa(\frac{\partial T_a}{\partial z}+\Gamma)] \qquad (2.1)$$

where T_a is the air temperature, κ is the thermal diffusivity, z is the height in vertical direction, and Γ is the advection term. For ground heat flux in soil, the advection term is negligible, thus the diffusion equation can be expressed as:

$$\frac{\partial T_s}{\partial t} = \frac{\partial}{\partial z_s}\left(\kappa_s \frac{\partial T_s}{\partial z_s} \right) \qquad (2.2)$$

where T_s is the surface temperature, z_s denotes depth and κ_s is the thermal diffusivity in soil. The substitution $z_s = \zeta_s \sqrt{\kappa_s}$ and $z = \zeta\sqrt{\kappa}$ can reduce all media to a common basis, so that in any condition the depth of penetration is proportional to $\sqrt{\kappa_s}$ or $\sqrt{\kappa}$. That is to say, the rate of heat flux consequent on an imposed temperature at the boundary will be directly proportional to $\rho_s C_s \sqrt{\kappa_s}$, where $\rho_s C_s$ is the heat capacity of the soil medium. And this relationship is independent of time. With T_s in equation (2.2) the counterpart of $(T_a + \Gamma z)$ in equation (2.1), the conditions in two media are the same except that κ differs from κ_s. Assuming the values of κ and κ_s are constant, in the case of a simple harmonic source of heat at the boundary, the relative efficiency between G and H can be obtained:

$$\frac{H_0}{G_0} = \frac{\rho C_p \kappa (\frac{\partial T_a}{\partial z} + \Gamma)}{\rho_s C_s \kappa_s (\frac{\partial T_s}{\partial z_s})} = \frac{\rho C_p \sqrt{\kappa}(\frac{\partial T_a}{\partial \zeta} + \Gamma\sqrt{\kappa})}{\rho_s C_s \sqrt{\kappa_s}(\frac{\partial T_s}{\partial \zeta_s})} = \frac{\rho C_p \sqrt{\kappa}}{\rho_s C_s \sqrt{\kappa_s}} \qquad (2.3)$$

where ρ is the density of air, ρ_s is the bulk density of soil, C_p is specific heat of air, and C_s is the specific heat of soil. From equation (2.3) one can conclude that the relative efficiency of ground heat flux in Priestley model is determined by the

thermal properties of media themselves, at all times and irrespective of the form of the time variation imposed at the boundaries. For soil and air layer, typical values of the relevant properties can be founded in references.

Latent heat flux is the heat that released or absorbed by a body during a process that occurs without a change in temperature. Generally the latent heat can be given by:

$$LE = L_V \times E \tag{2.4}$$

where E is the evaporation rate, $L_V = 2260 kJ/Kg$ is the latent heat of vaporization. Note that L_V will change with different substances. The evaporation term E had been discussed by several researchers by the time Priestley developed the classical model (Thornthwaite and Holzman 1939; Pasquill 1949; Deacon and Swinbank 1956). Since high frequency measurements were not available at that time, one common property of all these proposed methods was that E is determined by the specific humidity, wind velocity and height data from two measurement heights. Assuming the eddy-transfer mechanisms are identical for T and q, H and LE will have a similar mathematical form except that multiplying coefficient will be different. The relationship between H and LE can be expressed as:

$$\frac{LE}{H} = \frac{C_p}{L_V} \frac{T_2 - T_1}{q_2 - q_1} \tag{2.5}$$

Over saturated surface, a number of workers had attested that equation (2.5) provides satisfactory estimates of relation between LE and H. In drier conditions, field measurements by Pasquill (1949) and Swinbank (1955) had

12

failed to corroborate equation (2.5). Thus in this study, Priestley model is only applied to saturated surface condition. Surface water availability parameter is not introduced into Priestley model as in LSA model and MEP model.

For a saturated surface, the specific humidity can be computed using the Clausius-Clapeyron relationship:

$$q_s^*(T) = \frac{\xi e_s^*(T)}{p} = \frac{\xi e_0}{p} exp\left[\frac{\lambda}{R_V}\left(\frac{1}{T_0} - \frac{1}{T}\right)\right] \tag{2.6}$$

where $q_s^*(T)$ is the saturated specific humidity at temperature T in Kelvin, ξ is the ratio of dry air to water vapor gas consant and equals to 0.622, p is the atmosphere pressure, $e_s^*(T)$ is the saturated vapor pressure at T, T_0=273.15K and e_0 is a reference condition of vapor pressure ($e_0 = 611pa$), λ is the latent heat of vaporization at T_0 ($\lambda = 2.495 \times 10^6 \, J/kg$) and R_V is the gas constant for water vapor ($R_V = 463J/(K * Kg)$). The variation of $q_s^*(T)$ with air temperature is shown in Figure 2.2.

It is shown in Figure 2.2 that q_s^* profile is a curve with respect to air temperature. However, with the assumption that diurnal range is small enough, q_s^* can be taken as a linear function of T_a (hypotenuses in Figure 2.2). Then, to the extent that the mechanisms for vertical diffusion of heat and vapor are the same everywhere, the relative efficiency of *LE* to *H* will become:

$$\frac{LE}{H} = \frac{C_p}{L_V}(\frac{\partial q_s^*}{\partial T})_{T=Ts} \tag{2.7}$$

As shown in Figure 2.2, the slope of q_s^* curve will increase with air temperature, thus the relative efficiency of latent heat flux is also expected to increase with air temperature.

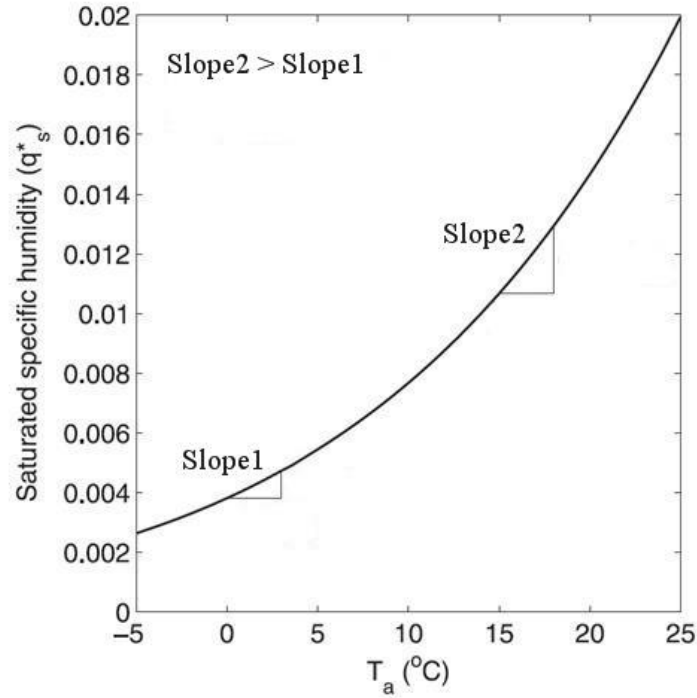Figure 2.2. Variation of saturated specific humidity with air temperature

2.2 Linear stability analysis

One-dimensional vertical heat diffusion equation can be expressed as:

$$\rho_s C_s \frac{\partial T_s(z,t)}{\partial t} = \kappa \frac{\partial^2 T_s(z,t)}{\partial z^2} \qquad (2.8)$$

With boundary conditions:

$$\lim_{z \to \infty} T_s(z,t) = \bar{T}$$

$$-\kappa \frac{\partial T(0,t)}{\partial z} = G(t) \qquad (2.9)$$

where κ is the thermal diffusivity, $T_s(z, t)$ is the soil temperature at depth z and time t, $\bar{T}$ is the deep ground temperature, $G(t)$ is the ground heat flux varying with time. Rearranging equation (1.2) one can easily get:

$$G = R_n - H - LE \qquad (2.10)$$

Each flux term on the right-hand side of equation (2.10) is generally related to the surface temperature and restores the system to equilibrium. The solution to equations (2.8) and (2.9) may be approximated at the surface by a single ordinary differential equation, which is well known as the force-restore equation. The force-restore method is a two-layer approximation where a shallow slab of soil near the surface is bounded below by a thick constant-temperature slab (see Figure 2.3). This method allows modeling the evolution of surface temperature response to variations in *G(t)* at a principal diurnal frequency. The approximation needs the following assumptions: (1) the ground heat flux *G(t)* has a strong diurnal behavior; (2) soil thermal properties are nearly constant with depth (Dickinson 1988). Using the force-restore-method, equation (2.10) can be expressed as:

$$\frac{dT_s}{dt} = \frac{\sqrt{\omega}}{P}(R_n - H - LE) - \omega(T_s - \bar{T}) \qquad (2.11)$$

where ω is the diurnal frequency, *P* is the thermal inertia.

15
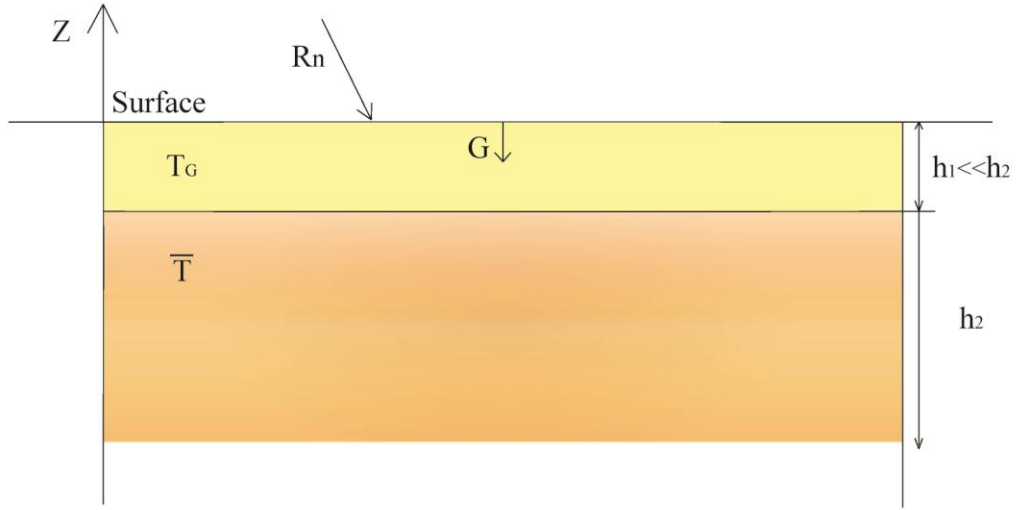
Figure 2.3. Schematic of force-restore method

The first term on the right-hand side is the forcing term, which accounts for the diurnal behavior of surface energy budgets. And the second term is the restoring term for considering the deep soil temperature. Based on this equation, Bateni and Entekhabi (2012) used further simplifications and developed the linear stability analysis method for deriving relative efficiency of surface energy budget components.

In the view of spectrum, net radiation in equation (2.11) can be expressed in terms of shortwave and longwave radiation:

$$R_n = (1-\alpha)S\downarrow + L\downarrow - L\uparrow \qquad (2.12)$$

where α is the surface albedo, S and L are respectively shortwave and longwave radiation, arrow stands for the direction of the radiation. Generally, $L\uparrow$ is approximated by:

$$L\uparrow = \varepsilon\sigma T_s^4 + (1-\varepsilon)L\downarrow \qquad (2.13)$$

16

where ε is the emissivity and $\sigma = 5.67 \times 10^{-8} (W/m^2 K^4)$ is the Stefan-Boltzmann constant. For most surface types, emissivity is close to 1, thus the contribution of incoming longwave radiation to the outgoing longwave radiation is negligible. In this model, outgoing longwave radiation is given by:

$$L\uparrow = \varepsilon \sigma T_S^4 \tag{2.14}$$

Using a bulk resistance formulation, sensible heat flux is computed by:

$$H = \frac{\rho C_p}{r_a}(T_s - T_a) \tag{2.15}$$

where T_a is the air temperature at a reference height, and r_a is the aerodynamic resistance for heat transfer from surface to the air layer at the reference height.

In the case of moist soil or well-watered vegetation, the maximum latent heat flux can be obtained by potential evaporation:

$$LE_P = \frac{\rho L_V}{r_a}(q_s^*(T_s) - q_a) \tag{2.16}$$

where q_a is the specific humidity at the overlying air layer. To obtain the actual evaporation rate from the potential evaporation, a moisture availability parameter β is introduced by Bateni and Entekhabi (2012). β is dependent on soil moisture or vegetation stress and links the energy balance to the water balance. It should be noted that β is a bulk parameter here to indicate the conditions where evaporation is below its potential value. The actual latent heat can then be expressed by:

$$LE = \beta \times LE_P \tag{2.17}$$

Substituting equation (2.14) to (2.16) into equation (2.11) results in

$$\frac{dT_s}{dt} = \frac{\sqrt{\omega}}{P}[(1-\alpha)S\downarrow +L\downarrow -\varepsilon\sigma T_S^4 - \frac{\rho C_p}{r_a}(T_s - T_a)$$
$$-\beta\frac{\rho L_V}{r_a}(q_s^*(T_s)-q_a)] - \omega(T_s - \overline{T})$$

(2.18)

As shown in equation (2.18), all flux terms are functions of T_s and T_a. The system requires measurements of two temperatures to determine the dissipative fluxes, thus the next step is to simplify the mathematical expression for all fluxes that the relative efficiency can be expressed in terms of only one temperature. Since solar radiation is applied to the surface, dissipative fluxes are affected by surface temperature thus it will be better to simplify the flux terms into a single function of T_S. Taylor's series can help this process to linearize T_s around T_a, the mathematical expression of Taylor's series is:

$$f(x) = \sum_{n=0}^{\infty}\frac{f^{(n)}(a)}{n!}(x-a)^n$$

(2.19)

where a is a neighborhood of x. Using the truncated Taylor's series, outgoing longwave term $(\varepsilon\sigma T_S^4)$ and saturated specific humidity $(q_s^*(T_s))$ are linearized around air temperature and become a linear function of surface temperature:

$$\varepsilon\sigma T_S^4 = -3\varepsilon\sigma T_a^4 + 4\varepsilon\sigma T_a^3 T_s$$

(2.20)

$$q_s^*(T_s) = q_s^*(T_a) + \frac{\partial q_s^*}{\partial T_s}\Big|_{T_s}(T_s - T_a)$$

(2.21)

After using the truncated Taylor's series, all the flux terms in equation (2.11) become linear functions of T_S with different orders of T_a. Assuming surface temperature and air temperature are in two separate systems that they do

18

not have strong relationships with each other, substitute equation (2.20) and (2.21) into equation (2.18) will yield:

$$\frac{dT_s}{d\tau} = -\left(\beta \frac{\Delta}{\gamma} T_s + T_s + \frac{r_a}{r_0} T_s + \frac{r_a}{r_g} T_s \right) + Q' \tag{2.22}$$

where τ is the nondimensional time scale:

$$\tau = \frac{\rho C_p \sqrt{\omega}}{pr_a} t \tag{2.23}$$

Δ is the Clausius-Calpeyron relation:

$$\Delta = \frac{de_s}{dT_s} \tag{2.24}$$

γ is the Psychometric constant:

$$\gamma = \frac{C_p p}{0.622 L_V} \tag{2.25}$$

r_0 is the radiative flux resistance:

$$r_0 = \frac{\rho C_p}{4 \varepsilon \sigma T_a^3} \tag{2.26}$$

r_g is the ground heat flux resistance:

$$r_g = \frac{\rho C_p}{P \sqrt{\omega}} \tag{2.27}$$

And Q' is the complexity of state variable:

$$Q' = \frac{(1-\alpha) S \downarrow + L \downarrow}{\rho C_p / r_a} + \left(1 + \frac{3 r_a}{4 r_0} \right) T_a - \beta \frac{L_V}{C_p} q_s^*(T_a) + \beta \frac{L_V}{C_p} q_a + \beta \frac{\Delta}{\gamma} T_a + \frac{r_a}{r_g} \overline{T} \tag{2.28}$$

In equation (2.22), four terms in the bracket from left to right respectively stands for *LE*, *H*, *OLR* and *G*. From the negative sign it can be concluded that the

19

system is always dissipative. By this approach, all these flux terms can be regarded as a linear function of T_s and relative efficiency of them can then be independent of T_s. It should be noted that two important dependencies have been neglected in this linearization. First, the gradients in air temperature will affect the static, buoyancy and ultimately turbulence in the stability. The model does not explicitly contain this dependence. Second, ground heat flux resistance r_g varies with volumetric moisture content in the soil slightly. This dependence is also not factored in the model.

On a daily scale, the system tends to restore to an equilibrium temperature T_S^*, writing equation in terms of deviation from T_S^* will yield:

$$\frac{d(T_s - T_S^*)}{d\tau} = -\left(\beta \frac{\Delta}{\gamma} + 1 + \frac{r_a}{r_0} + \frac{r_a}{r_g}\right)(T_s - T_S^*)$$ (2.29)

The solution to equation (2.29) is:

$$\delta T_s(\tau) = \delta T_s(0) e^{-\beta \frac{\Delta}{\gamma}\tau} e^{-\tau} e^{-\frac{r_a}{r_0}\tau} e^{-\frac{r_a}{r_g}\tau}$$ (2.30)

where $\delta T_s(\tau)$ is the surface temperature perturbation, $\delta T_s(0)$ is the initial perturbation due to anomalies as included in Q'. From equation (2.30) the relative efficiency of different flux terms is obtained:

$$\begin{cases} \dfrac{LE}{H} = \beta \dfrac{\Delta}{\gamma} \\[2mm] \dfrac{OLR}{H} = \dfrac{r_a}{r_0} \\[2mm] \dfrac{G}{H} = \dfrac{r_a}{r_g} \end{cases}$$ (2.31)

2.3 Maximum entropy production

An alternative way to derive the relative efficiency, from thermodynamic

principles, is to use the maximum entropy production (MEP) theory. The

constrained maximization of Shannon information entropy (MaxEnt) is an

algorithm for constructing probability distribution from partial information, which

can serve as a statistical tool of considerable generality. Dewar (2005) presented a

rigorous and general mathematical derivation of maximum entropy production

(MEP) from MaxEnt and clarified the relationship between MEP and fluctuation

theorem (FT). Based on the MEP theory, Wang and Bras (2009, 2011) developed

surface heat fluxes and evaporation models from which the energy partitioning

into different fluxes can be determined.

In the MaxEnt formulation, the probability p_i of variable x_i is derived

by maximizing the Shannon information entropy S_I:

$$S_I = -\sum_{i=1}^{n} p_i \ln(p_i) \tag{2.32}$$

subject to the constraints:

$$\sum_{i=1}^{n} p_i f_k(x_i) = F_k, \qquad 1 \le k \le m \tag{2.33}$$

where f_k is the function of x_i, F_k is the given parameter representing available

information about x_i, and $m \ll n$ is a given integer. Using the Legendre

transform will lead to:

$$p_i \propto exp\left[\sum_{k=1}^{m} \lambda_k f_k(x_i)\right] \tag{2.34}$$

21

where λ_k are the Lagrange multipliers associated with the constraints, $F_k (1 \le k \le m)$. The MEP theory results from the particular situation where f_k in equation (2.34) is anti-symmetric function satisfying $f_k(x_{i+}) = f_k(x_{i-})$ when the variable x_i can be grouped in pairs (i_+ , i_-). And for anti-symmetric function f_k, the corresponding MaxEnt distribution satisfies the generic "fluctuation theroem" :

$$\frac{p_{i+}}{p_{i-}} = exp\left[\sum_{k=1}^{m}\lambda_k f_k\left(x_{i+}\right)\right] \tag{2.35}$$

Unless the bracket term in equation (2.35) is always close to zero, the left-hand side of equation (2.35) will not be equal to 1, which means the macroscopic transport of heat exists due to the anti-symmetry. From equations (2.34) and (2.35), one can easily find that the anti-symmetric function is determined by the properties of the exponent of the exponential function in equation (2.35), which is referred as the "dissipation function" and its mathematical expectation is:

$$D = 2\sum_{k=1}^{m}\lambda_k F_k(x_i) \tag{2.36}$$

Since there is a negative sign on the right-hand side of equation (2.32), maximizing the Shannon information entropy S_I actually equals to minimizing p_i. And from the dissipation function, minimizing p_i equals to minimizing D. D is maximum when the constraint F_k is a certain nonlinear function, and minimum when F_k is a linear function. Therefore, MEP in fact depends on the functional expression of the constraints. And the key to apply the MEP is to

obtain an expression of D where λ_k is expressed as explicit functions of F_k according to the Legendre transformation once f_k is defined. In the case of heat exchange at the surface, f_k may include the kinetic energy of molecules or turbulent eddies, determining which requires the understanding of the physical process at a microscopic level. Yet the macroscopic observable properties are irrelevant to the most of the microscopic details which are hard to capture. Thus it is possible to find D without knowing f_k exactly.

Wang and Bras (2009) considered the condition where a source of heat is located at the ground surface between two semi-infinite column systems with its input R_n varying with time and developed a toy model (see Figure 2.4). Heat input to the surface will be dissipated by fluxes into those two columns according to the conservation of energy. F_1 and F_2 are heat fluxes from the boundary into the columns, F_0 is the total incoming energy. The fluxes are determined by minimizing:

$$D = \frac{2F_1^2}{I_1} + \frac{2F_2^2}{I_2} \tag{2.37}$$

Subject to the conservation of energy:

$$F_0 = F_1 + F_2 \tag{2.38}$$

An analytical solution of F_1 and F_2 is given by solving the diffusion equations:

$$F_k = \frac{I_k}{I_1 + I_2} F_0 \qquad k = 1, 2 \tag{2.39}$$

where I_1 and I_2 are the thermal inertias of the media separated by the surface.

λ_k in equation (2.36) is expressed as:

$$\lambda_k = \frac{F_k}{I_k} \qquad k = 1,2 \tag{2.40}$$

which is recognized as the orthogonality conditions by Dewar (2005). Detailed process of derivation can be found in Appendix A of the original paper (Wang and Bras 2009). Expressing the F_k in terms of surface temperature, the physical meaning of λ_k can be found (Wang and Bras 1999):

$$F_k = \frac{I_k}{\sqrt{\pi}} \int_0^t \frac{dT_s(\tau,0)}{\sqrt{t-\tau}} \qquad k = 1,2 \tag{2.41}$$
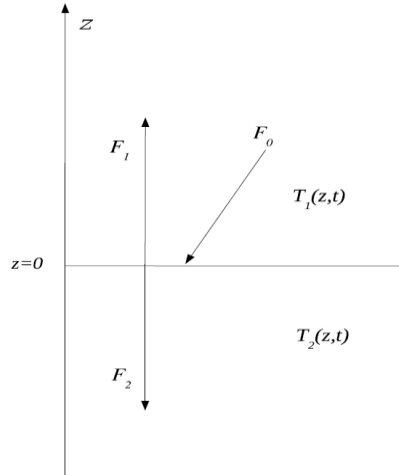

Figure 2.4. Schematic of the MEP model

Combining equation (2.40) and (2.41) λ_k is found to be half-order time derivative of the surface temperature. As time goes, a continuous distribution of temperature will happen through the two columns. Replace flux terms in equation (2.37) by *H*, *LE* and *G*, the model becomes:

$$D = \frac{2G^2}{I_G} + \frac{2H^2}{I_H} + \frac{2LE^2}{I_{LE}}$$ (2.42)

subject to:

$$R_n = H + LE + G$$ (2.43)

where I_G, I_H, I_{LE} are the thermal inertia parameters for heat conduction

associated with corresponding fluxes. R_n here is a known variable. For the

ground heat flux, I_G should characterize the thermal property of the soil, as a

composition of density, specific heat and thermal diffusivity. A convenient

method for estimating I_G is given by Wang et al (2010). I_G is a well-defined

term given by:

$$I_G = \sqrt{\rho_s c_s / 2}$$ (2.44)

I_H is first introduced by Wang and Bras (2009). Theoretically, I_H is the

thermal inertia for turbulent heat transfer in the air. Assuming it has the same

composition with I_G, it needs the parameterization of eddy diffusivity in the air.

Monin-Obukhov similarity theory (Arya 1988) serves as a good basis for

modeling turbulent transport in the ABL. In the theory, eddy diffusivity is

expressed in terms of two of the four state variables, i.e., gradients of mean wind

velocity and temperature, heat fluxes and momentum fluxes. Wang used an

extremum solution based on the Monin-Obukhov similarity theory, reducing the

freedom from two to one thus I_H is formulated as a function of heat fluxes alone.

It should be noted that the extremum solution remove the nonuniqueness in the

relationships between gradient variables and flux variables in the theory, allowing

25

them to be expressed in terms of the other. Detailed process can be found in Appendix B of original paper (Wang and Bras 2009).

$$I_H = \rho C_p \sqrt{C_1 \kappa z} (C_2 \frac{\kappa z g}{\rho C_p T_0})^{1/6} |H|^{1/6} \tag{2.45}$$

where κ here is the von Karmen constant, T_0 is the reference temperature. C_1 and C_2 are coefficients related to the universal constants (α, γ_2, β) in the empirical functions representing the effect of the stability on the mean profiles of wind speed and temperature within the surface layer (Businger et al. 1971):

$$
\begin{aligned}
C_1 &= \begin{cases} \sqrt{3}/\alpha = 1.732, & \textit{unstable} \\ 2/(1+2\alpha) = 0.667, & \textit{stable} \end{cases} \\
C_2 &= \begin{cases} \gamma_2/2 = 4.5, & \textit{unstable} \\ 2\beta = 9.4, & \textit{stable} \end{cases}
\end{aligned}
\tag{2.46}
$$

The constants are respectively: $\alpha \sim 0.75$, $\gamma_2 \sim 9$, $\beta \sim 4.7$.

I_{LE} is the thermal inertia for latent heat, thus it should take into account the turbulent diffusion of water vapor and the movement of liquid water. The turbulent mixing responsible for heat transport in the air layer is also responsible for the transport of the water vapor, which implies a functional dependence of I_{LE} on I_H. Also, Wang et al. (2004) have shown that physics of evaporation allows a diagnostic relationship relating LE to the intensity of turbulence characterized by fluxes of sensible heat or momentum. Based on this, I_{LE} is estimated by:

$$I_{LE} = \sigma I_H \tag{2.47}$$

where σ is a function justified by limiting cases of dry and saturated soil. For the dry soil, evaporation is totally eliminated that $\sigma=0$, and for the saturated soil, σ is given by:

$$\sigma = \frac{\Delta}{\gamma} = \frac{\lambda^2 q_s}{C_P R_V T_S^2} \tag{2.48}$$

Δ and γ are the same as defined in LSA model, Δ is the slope of saturation water vapor pressure curve at T_S. σ is the term describing the soil water availability related to the surface temperature (see Figure 2.5). Since the relation between exact σ value and soil water availability is not explicitly explained, this study incorporates the parameter β described in LSA model into the MEP theory as a scale parameter. β here represents the ratio of actual σ to the maximum σ value, increasing from 0 to 1 when soil condition changing from dry to fully saturated condition. After substituting all the thermal inertias into equation (2.42) and (2.43), the relative efficiency of fluxes can be obtained:

$$\frac{LE}{H} = B(\sigma) = 6\left(\sqrt{1 + \frac{11}{36}\sigma} - 1\right) \tag{2.49}$$

$$\frac{G}{H} = \frac{B(\sigma)}{\sigma} \frac{I_G}{I_H} \tag{2.50}$$

As shown in Equation (2.48), σ is a function of the surface temperature. Since σ is included in equation (2.49) and (2.50), relative efficiency of dissipative fluxes in MEP theory will also vary with surface temperature, the variation is shown in Figure 2.5. It is shown that the relative efficiency of latent

27

heat increases rapidly with surface temperature while the relative efficiency of

ground heat flux is relatively insensitive to the change in surface temperature.

For vegetated land surface, the MEP model of transpiration may be

viewed as another limiting case of the MEP formulation discussed above. In this

case, the energy balance is defined at the leaf surface that G here is understood as

the heat flux downward from the surface of the leaf. Consequently, if the plants

are short and closed to the surface, G can be defined as the same in the models

above. Over vegetation surface, the solution to equations (2.42) and (2.43) will

exactly yield the same relative efficiency as shown in equation (2.49) and (2.50),

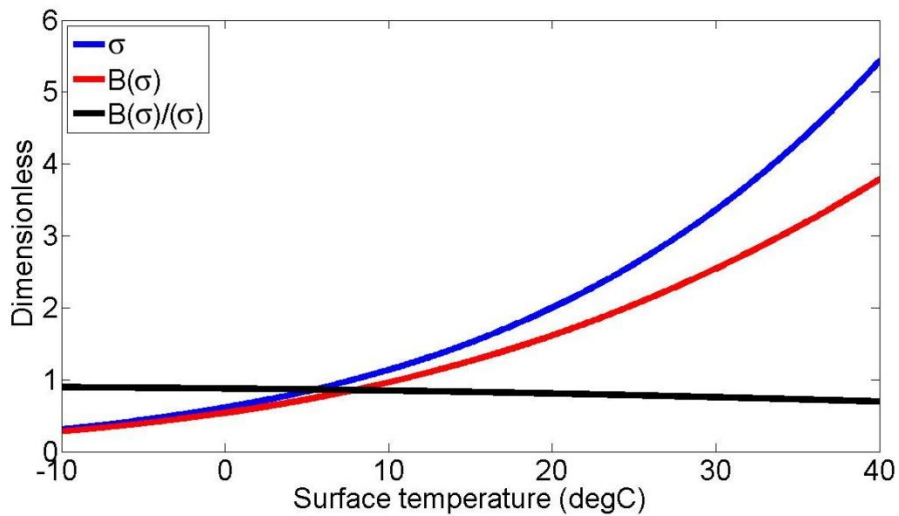except that T_s and q_s represents leaf temperature and specific humidity at the leaf

surface.

Figure 2.5. Variation of soil water availability and relative efficiency with surface

temperature

Chapter 3

EXPERIMENTAL OBSERVATION

One of the motivations of this study is to develop mitigation strategies for urban heat island effect. It is well known that, white roofs can reduce the sensible heat by increasing the outgoing longwave radiation, while green roofs can reduce the sensible heat through evaporation and increase of the latent heat. Different land covers will result in different relative efficiencies of surface energy budgets. Thus it is desirable to obtain the relative efficiency over frequently used urban land covers, based on which the mitigation of a specific turbulent flux can be achieved dependent on designer's purpose. To determine the relative efficiency of turbulent fluxes over frequently used pavements, field measurements are needed to estimate the fluxes. Before installing the eddy covariance towers, simple wireless stations with a set of sensors are deployed to verify the differences between different land covers first.

Figure 3.1. Google map of sensor network sites (5 stations at point A and two stations at point B)

Figure 3.2. Field view of experiment setup over different urban land covers

      The experiment site is located on Curry Road, north of the Arizona State University (ASU) Tempe campus, in Arizona (see point A in Figure 3.1). In sum six types of pavements are deployed on the experiment site, respectively, gravel, green turf, concrete, porous concrete, asphalt and porous asphalt (See Figure 3.2). A set of sensors is attached to a tube and deployed over each pavement, measuring the meteorology data (standard setup is shown in Figure 3.3). Air temperature and humidity sensors (Decagon) are located at 3 ft and 5 ft high respectively. Surface temperature is measured by Infrared guns (TNX). Besides, solar radiation is measured by radiometers (Davis), wind speed and directions are measured by cup anemometers (Davis) and precipitation is measured using tipping buckets (Davis). All sensors are synchronized and data is sampled every 1 minute. At last the data is collected by the wireless stations and uploaded to the internet automatically every 20 minutes. Measurement starts from September 6, 2012 and is still underway at the time when this study is presented.

Figure 3.3. Experimental set-up for each urban land cover

Time series plots of the data from the experiment site are shown in Figure 3.4 for a week. For the station numbers in the graph, station 1296 stands for porous asphalt surface, 1324 is over gravel surface, 1325 is over green turf surface, 1327 is over porous concrete surface, 1328 is over concrete surface and 1329 is over asphalt surface. From Figure 3.4(a), one can find significant deviation in surface temperature over different pavement types. The maximum surface temperature is found at the green turf and the minimum is at the concrete surface, with a maximum difference of about 18℃. However, it is shown in Figure 3.4(b) that the air temperature at 5 ft high over different land covers are almost identical, with a maximum difference of about 3℃. This result indicates that the existence of turbulent eddies near the surface makes the temperature in the air layer almost independent of the direct underlying surface. It also proves

31

that the separation of air temperature and surface temperature in linear stability

analysis model is reasonable.

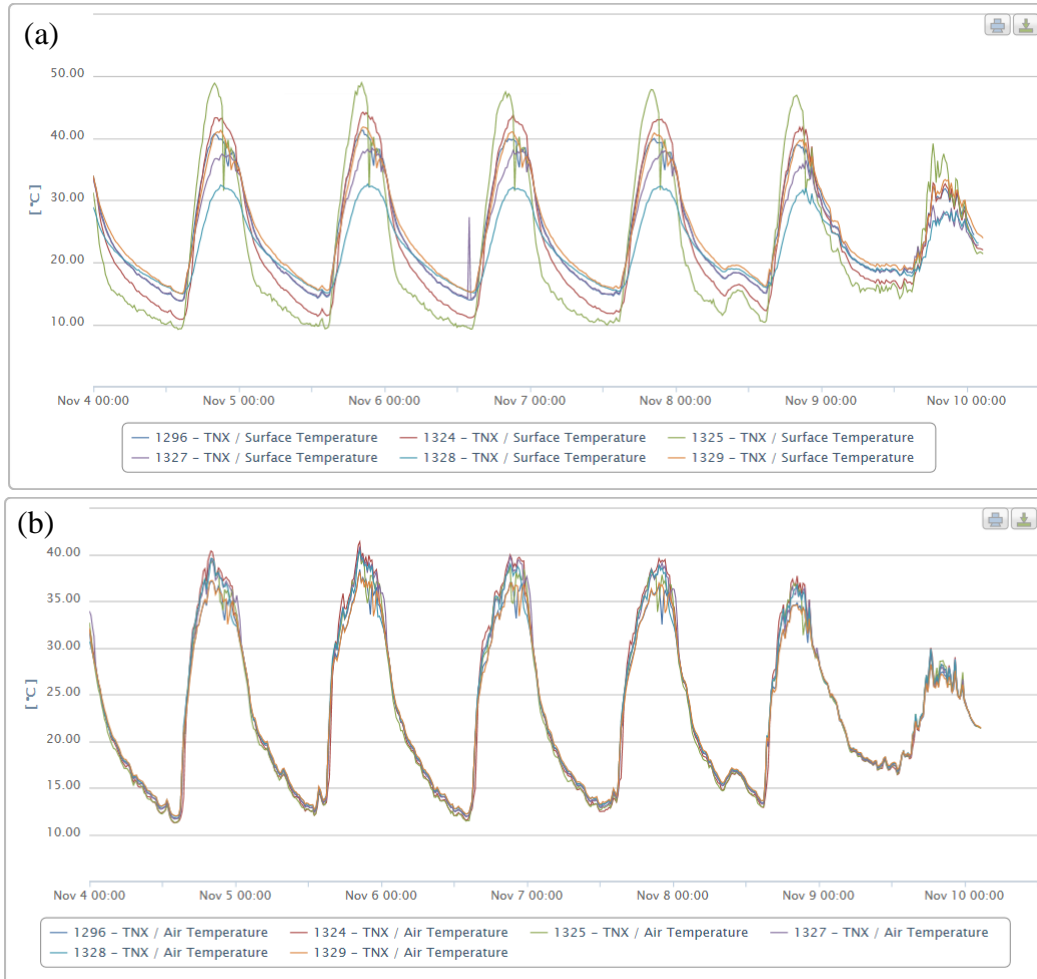Figure 3.4. Time series of temperature over frequently used urban land covers: (a)

surface temperature (b) air temperature

This experiment is part of the sensor network project by Urban Climate

Research Group at Arizona State University. Two other wireless stations are

deployed on the same roof on the ASU campus (see point B in Figure 3.1).

Currently this project is still under way and future stations are planned.

Chapter 4

DATA COLLECTION AND PROCESSING

4.1 Data collection

For verifying different methods of relative efficiency discussed above, data needs to be collected for analysis. In this study, three EC datasets over different land covers were collected, respectively, grassland, lake and suburban area. The station set-up and site condition of each experiment is briefly described below.

4.1.1   Lake data

The lake data used in this study was collected during the time period 15 August to 27 October 2006, shared by the Environmental Fluid Mechanics and Hydrology Laboratory at the Swiss Federal Institute of Technology-Lausanne, detailed information can be found in the original paper (Vercauteren et al. 2008, 2011). A 10-m high eddy covariance tower was installed to carry out the measurement. The tower was located 100m away from the northern shore of Lake Geneva in Switzerland (42.6 °N, 88.4 °W), in a shallow part of the lake about 4 m depth without significant aquatic vegetation (see Figure 4.1). Sensors were arranged as a vertical array to measure the data at four different heights, respectively, 1.66m, 2.31m, 2.96m and 3.61m (see Figure 4.2).
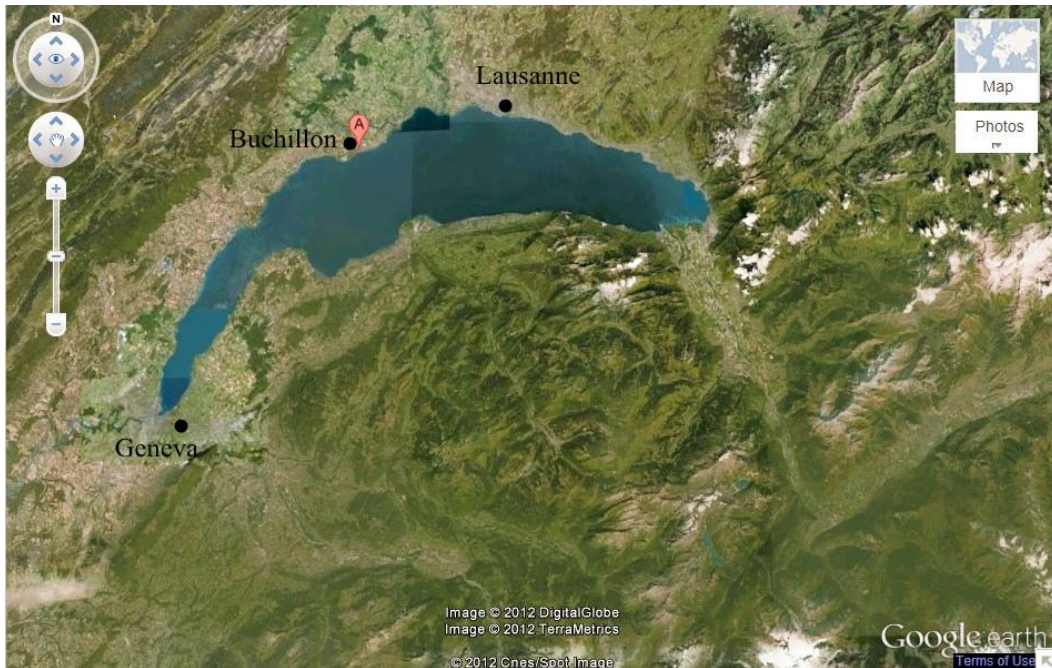
Figure 4.1. Google map of tower site (point A) in Lake Geneva, Switzerland

Sonic anemometers (Campbell Scientific CSAT3) and open-path gas analyzers (LICOR LI-7500) were used to measure air temperature, wind speed and humidity. Lake surface temperature was obtained by infrared thermocouple sensor (Apogee Instruments IRTS-P) and net radiation was measured by supporting sensor (Kipp&Zonen NR-Lite). Raw data were collected at 20 Hz using a Campbell Scientific CR5000 data logger and pre-processing was done before estimating fluxes. All instruments were intercompared in the laboratory for calibration before installing in the field. Under zero wind conditions, the errors from the sensors were recorded and they were used later as correction to field measurements. It should be noted that these corrections are improving the data quality and will not have a significant impact on the results. Because of technical issues, two gaps of 8 and 3 days existed in the dataset.

Figure 4.2. Experimental set-up of vertical arrays

4.1.2   Grassland data

In this section, experimental data over grassland was collected and shared by the Princeton Hydrometeorology Research Group. A standard eddy-covariance station was installed to measure the energy budgets over the field, which was covered by short grass (see Figure 4.3). Sonic anemometer (Campbell Scientific CSAT3), open path infrared gas analyzer (Licor Biogeosciences LI-7500), temperature and relative humidity probe (Vaisala) and four-component radiometer (Hukseflux) were used, collecting data at 10 Hz frequency. Besides the station, two sets of sensors were deployed for measuring ground heat fluxes (HFP01 heat flux plates), the soil temperature (TCAV thermocouple) and moisture content (CS616 water content reflectometer). Following the standard setup, the flux plats were placed at a depth of 8cm. And soil temperature was measured and spatially

35

averaged between 2cm and 6cm below the surface, sampled every 5 minutes. Detailed information can be found in the original paper (Wang and Bou-Zeid 2012).

Figure 4.3. Location and site condition of eddy covariance tower over grassland

4.1.3   Suburban data

Suburban data used in this study was collected and shared by the Environmental Fluid Mechanics Group at Princeton University. The Sensor Network Over Princeton (SNOP) project has been measuring continuous eddy covariance meteorological data for 2 years. SNOP includes a wireless network of 12 Sensorscope stations and conventional eddy-covariance stations deployed on the roof of buildings (see Figure 4.4). Detailed information can be found in the original paper (Wang et al. 2011). The experiment measured the data as over the footprint of suburban area.
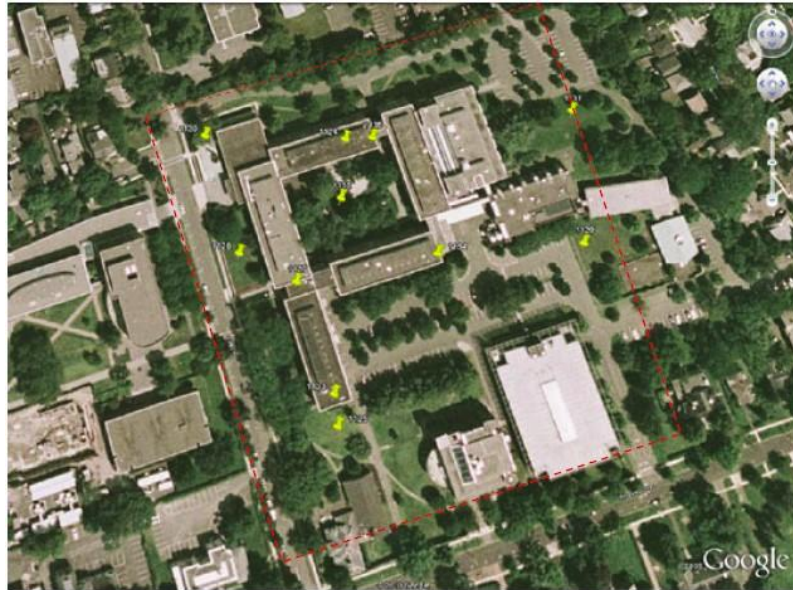
Fig 4.4. Google map of the measurement area (red dashed region) and station locations (yellow pointers), adopted from original paper (Wang et al. 2011)

For each Sensorscope station, a set of sensors were installed (see Figure 4.5), TNX infrared thermometer (ZyTemp) for surface temperature, a solar radiation sensor (Davis), and EC-TM probe (Decagon Devices, Inc) for volumetric water contents and soil temperatures. Eddy-covariance station consisted of three-dimensional sonic anemometer (CSAT3, Campbell Scientific), open-path infrared gas analyzer (LI-7500 from Licor Biogeosciences), temperature and relative humidity probe (HMP45C from Vaisala), infrared surface temperature recorder (IRR-P from Apogee Instrument), wind monitor (95193 R.M. Young from Campbell) and four-component radiometer (NR01 from Hukseflux).

Figure 4.5. Experimental set-up of Sensorscope station over suburban area

4.2 Data processing

4.2.1   Measurement correction

After collecting the data from different research groups, several processes are needed before using the data to estimate the turbulent fluxes. A standard data processing for high frequency eddy covariance dataset includes linear detrending, coordinate rotation and density correction. In this section they are briefly explained.

The eddy covariance method of calculating turbulent fluxes requires the fluctuating components of the measured signals which were derived by subtracting real time signals from the mean signals. For the mean signals, there may be a background trend caused by sensor drift or concentration. In steady state conditions simple linear means may be good, however, in atmospheric boundary

layer (ABL) steady state conditions rarely exist. Thus it is necessary to remove

this longterm trend in the data which does not contribute to the fluxes. The data

will first be divided into groups long enough to contain all the eddies transferring

the fluxes, usually 30 minutes, and a linear regression of the data is then

calculated. At last the fluctuations with respect to the regression line are

computed as the fluctuating components of the measured signals. Linear

detrending is such a process that gives improved estimation of fluxes and

variances with eddy covariance data.

In field observations, it has been well known that relatively small errors in

the alignment of turbulent wind sensors can lead to large errors in the

measurement of horizontal momentum flux (Pond 1968; Kaimal and Haugen

1969). These errors are due to the cross contamination of velocities in a tilted

sensor. To obtain the exact momentum fluxes, methods have been developed for

determining the tilt angles and computing tile-corrected stresses. The first most

commonly used method, double rotation (DR), was proposed by Tanner and

Thurtell (1969). This method involves a series of two rotations: first set $\bar{v} = 0$

by swinging x and y-axes around z-axis; second set $\bar{w} = 0$ by swinging new x

and z-axes around y-axis. Finally x-axis is aligned with the mean wind sector and

the anemometer's orientation is in y-z plane. DR method performances

reasonably well, however, the error in $\overline{vw}$ can be of the same order as the true

stress if the error in the y-z plane is small. A third rotation was suggested by

McMillen (1988) to remove this ambiguity by making $\overline{vw} = 0$. The triple

rotation method (TR) adds in a new step that rotates new y and z-axes around

39

x-axis until the $\overline{vw} = 0$. Besides these two methods, another method, planar fit

method (PF), was developed by Steve Stage (1977). This method computes the

mean wind vector and stress tensor for each averaging interval in a coordinate

system where z-axis is perpendicular to the mean streamlines. The intermediate

winds and tensors is rotated that x-axis is along the mean wind and $\bar{v} = 0$.

Wilczak et al. (2000) compared these three commonly used methods and

suggested using the planar fit technique for sonic anemometer tilt correction. The

planar fit technique, which provides an unbiased estimate of the lateral stress and

reduces the run-to-run stress errors, is used in this study.

For eddy covariance measurement directly in the air, heat and water vapor

transfer will cause expansion of the air and affect the result of minor constituents'

density such as CO_2. When dealing with flux balances, total vertical fluxes are

needed including the turbulent fluxes as well as the mean vertical fluxes. The

variations in constituents' density will eventually lead to errors in heat fluxes,

which usually will be smaller than 10 percents for water vapor flux but can be

larger than the flux itself for CO_2 flux. The most commonly used method for

correcting the density due to heat and water vapor transfer is developed by Webb

et al. (1977, 1980), well know as 'Webb's correction'. The conclusion is drawn

by Webb that: if the measurements are sensing constituent relative to the dry air

component, no correction is needed; if relative to the total moist air, only

correction for water vapor flux is needed; if in unmodified in situ air, both water

vapor and CO_2 fluxes need corrections. Based on this conclusion, Webb's

correction is applied for both fluxes in this study.

4.2.2   Data selection

After going through all the corrections for eddy covariance data, the turbulent fluxes can be well estimated. However, further processing is needed based on the interest of this study. Focusing on the surface energy partitioning process of solar radiation, in this study, daytime data are selected for subsequent analysis. Besides the available incoming radiation, all the theoretic models were developed assuming unstable atmospheric conditions where the upward turbulent transport prevails, i.e. the ABL must be convective. Under convective conditions, the surface layer is dominated by buoyant turbulence generation and strong vertical mixing is guaranteed.

As shown in Figure 4.6(a), air temperature will exceed the surface temperature around noon time over the lake surface, which is recognized as the oasis effect (Stull 1998). Due to oasis effect, sensible heat around noon time will go downward that the convective condition is not satisfied. Meanwhile, strong evaporation from the lake leads to the upward latent heat flux around noon time. In this case, latent heat flux can be greater in magnitude than the solar radiation because of the additional energy from the downward warm air. Thus time periods with oasis effect over water surfaces need to be filtered. As shown in Figure 4.6(a), data within the two shaded areas are selected for computing the relative efficiency of surface energy budgets over the lake surface.
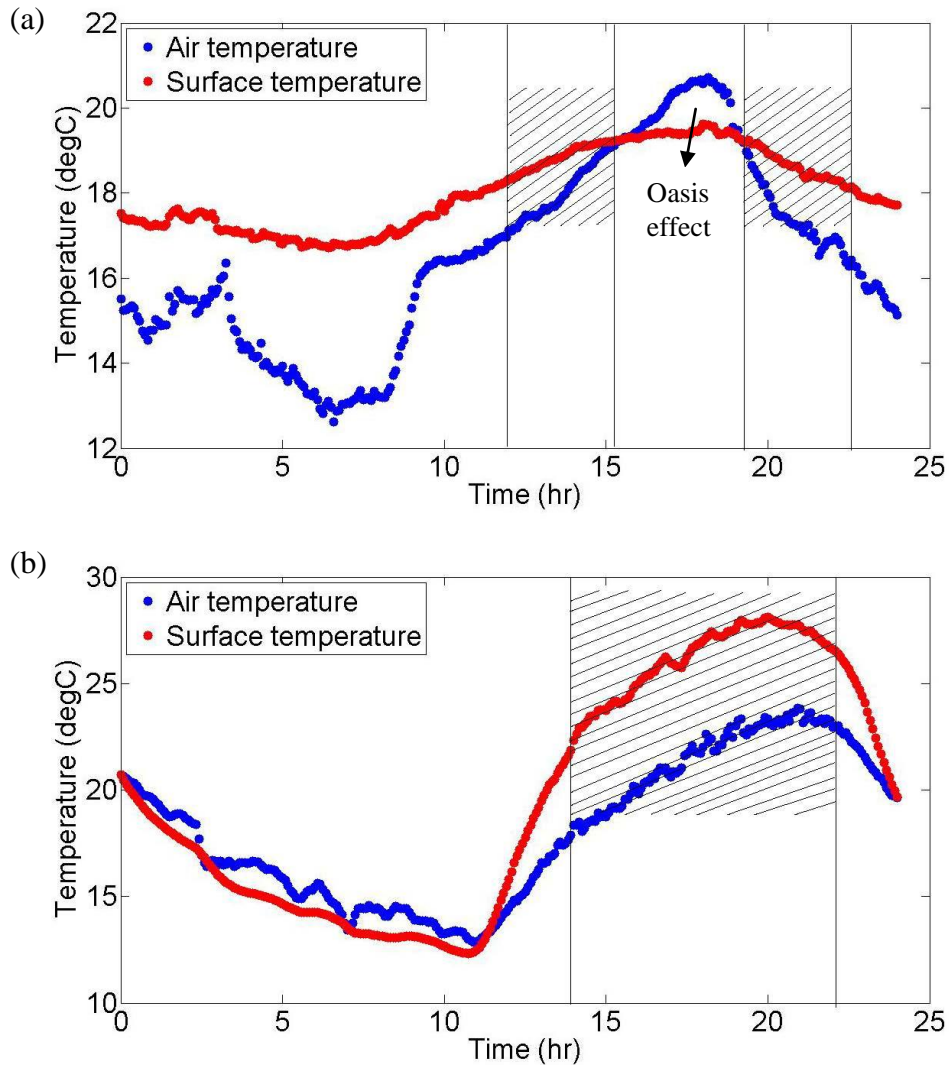
(a)

(b)

Figure 4.6. Data selection for different land covers during diurnal variation: (a) lake data (b) suburban and grassland data

For suburban area, the convective condition in surface layer is achieved during daytime. Data within the shaded area around noon time are selected for subsequent computation (see Figure 4.6(b)). Grassland data shows the same trend as suburban data thus the same period is selected. The daytime period will change as time shifts in the year, thus the selected time block is actually changing with respect to season. Furthermore, daily mean values for all surface energy budget

42

components, averaged over the selected period of convective conditions as

illustrated in Figure 4.6, were used in subsequent analysis to reduce the influence

of measurement errors.

Chapter 5

RESULTS AND DISCUSSION

5.1 Model prediction

Before verifying with field measurements, the intercomparison between

model results is carried out first. This intercomparison can help to find out the

similarities and differences between models, providing insights into the

mechanisms behind models. In this study the relative efficiency of turbulent flux

is defined as the ratio of the flux to the sensible heat for convenience. However,

this definition is not necessary and other fluxes can also be used as the

denominator of the ratio.

From Figure 5.1(a), it is shown that the relative efficiencies of latent heat

flux from the LSA model with different surface water availabilities are in similar

profiles. When β equals to 1, which means a saturated surface condition, result

from the LSA model is very close to that of Priestley model (see Figure 5.1(b)).

This is due to the use of the same aerodynamic resistance for estimating sensible

heat and latent heat in both models. And the specific humidity in both models is

computed based on the Clausius-Clapeyron relation, which leads to a close

evaporation rate. However, the classical method assumes $q_s^*(T)$ as a linear

function of air temperature, while in the LSA model $q_s^*(T)$ is a complicated

function. When air temperature increases, the different treatment will lead to
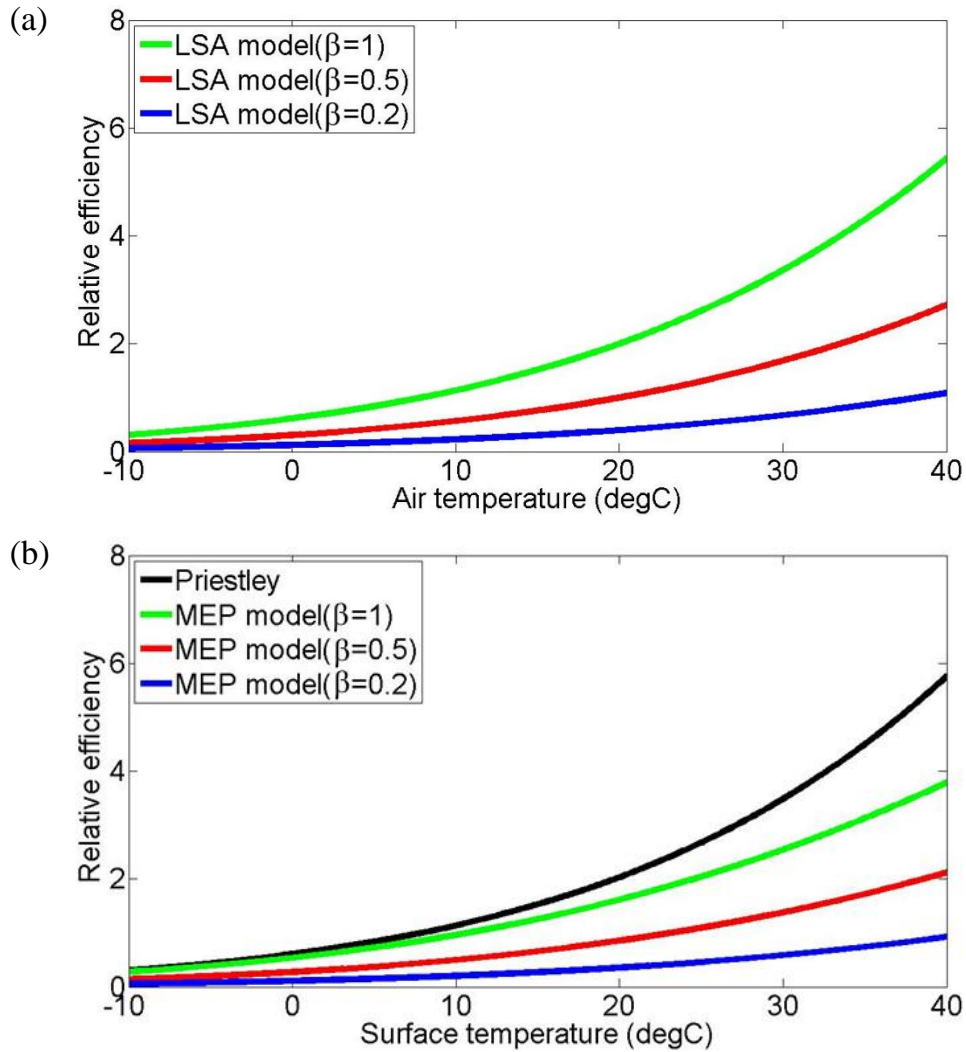
larger deviations.

Figure 5.1. Model predictions for relative efficiency of LE: (a) LSA model (b) MEP and Priestley model

In the LSA model, the relative efficiency is sensitive to the surface water availability parameter β. For low β values (<0.2), relative efficiency increases slightly from 0.1 to 1 when air temperature goes through a large rise from -10 ℃ to 40℃. For fully saturated condition ($\beta = 1$), relative efficiency increases significantly from 0.3 to 5.5 with the same temperature rise. The graph illustrates that for a given value of air temperature, the evaporation rate is at its peak when

the soil is fully saturated and the process is limited by available energy. As β

decrease, the condition becomes limited by water that evaporation decreases

rapidly. Compared to the LSA model, results from MEP theory are consistently a

little smaller at the same temperature. The increase in relative efficiency with

respect to β is smaller and the deviation from Priestley model is larger. However,

the trend is similar to that of the LSA model on the whole. Priestley model is

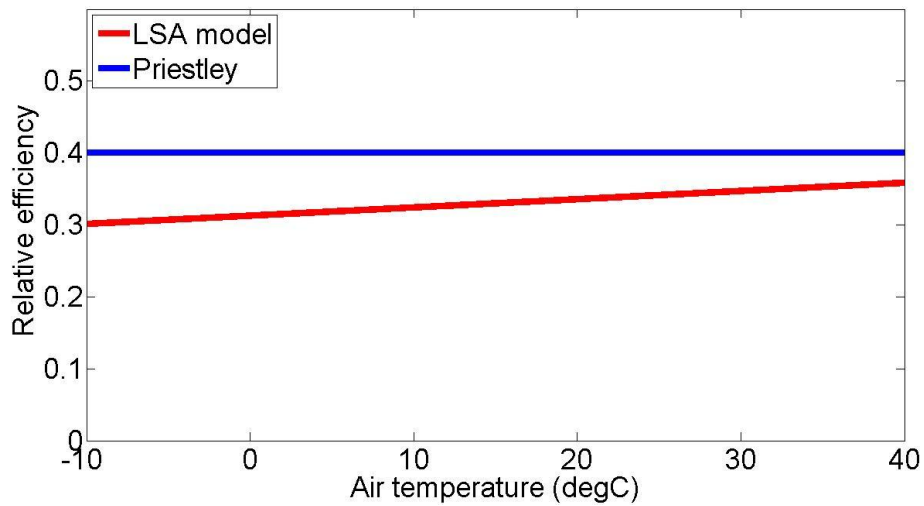predicting a larger relative efficiency than other two models over saturated

surface.

Figure 5.2. Model prediction for relative efficiency of G

For ground heat flux, field measurement is only available at the grassland

site. In Priestley model, the relative efficiency of *G* is indicated to be determined

by the thermal properties of the contacting media. Assuming constant properties,

Priestley model predicts the result to be a constant value 0.4 (see Figure 5.2). In

the LSA model, decrease of density is considered while the air temperature

increases, therefore the resulted profile goes through a slight increase with respect

to air temperature. For MEP theory, the result is not shown here since the relative

efficiency of *G* is a function related to *H*. Note that in the MEP model over

vegetation surface, the surface temperature is referring to the leaf temperature.

For outgoing longwave radiation, only the LSA model is able to predict

the relative efficiency. Result shows a slight increase about 0.2 in the relative

efficiency while air temperature rises from -10℃ to 35℃ (see Figure 5.3), which

is even smaller than that of *G*. The model indicates that energy partitioning into
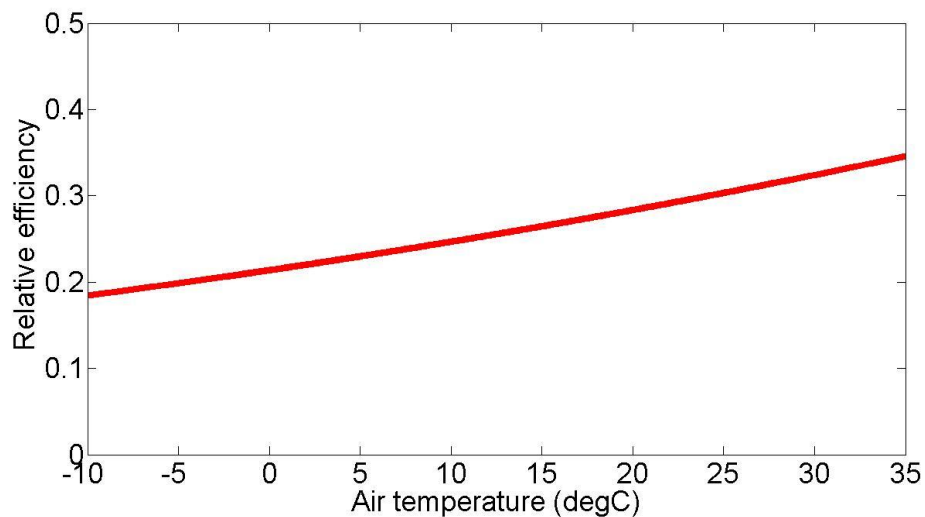
OLR is insignificant in normal temperature ranges.

Figure 5.3. Model prediction for relative efficiency of OLR

One important assumption needs to be pointed out is that r_a is set as a

nominal constant value for the LSA model in this study. Since the computation of

aerodynamic resistance is not feasible based on available data, r_a is set to be

60s/m according to the result from Bateni and Entekhabi (2012). This assumption

will certainly lead to discrepancies in the predictions of relative efficiency of *OLR*

and *G*. However, the performance of the LSA model can still be tested since

47

results are linear to r_a. Also, since no terms in model are accounting for the cloud and advection effect, the LSA model will perform the best under peak solar conditions with minimal advection.

5.2 Verification with field measurement

5.2.1 Latent heat flux

Model prediction of relative efficiency of *LE* over the suburban area is shown in Figure 5.4. Summer and winter are selected for analysis since weather conditions are significantly different in these two periods. In the LSA model, data concentrate in the range of β=0.05 to 0.3 for summer period (May to August). For winter period (November to February), same trend of data is observed but with a larger value of β from 0.1 to 0.7. As daily mean value is used in the analysis, generally parameter β is varying from day to day. However, for a specific season the value should concentrate within some ranges that represent the seasonal variability of the surface moisture. Deviations are shown in Figure 5.4, but they are within a reasonable range. Only 12% and 10% of field measurements are outside the predicted range, respectively in summer and winter. Indicated from the model results, more water is available at the surface in winter and it results in a higher relative efficiency at the same temperature compared to summer period.
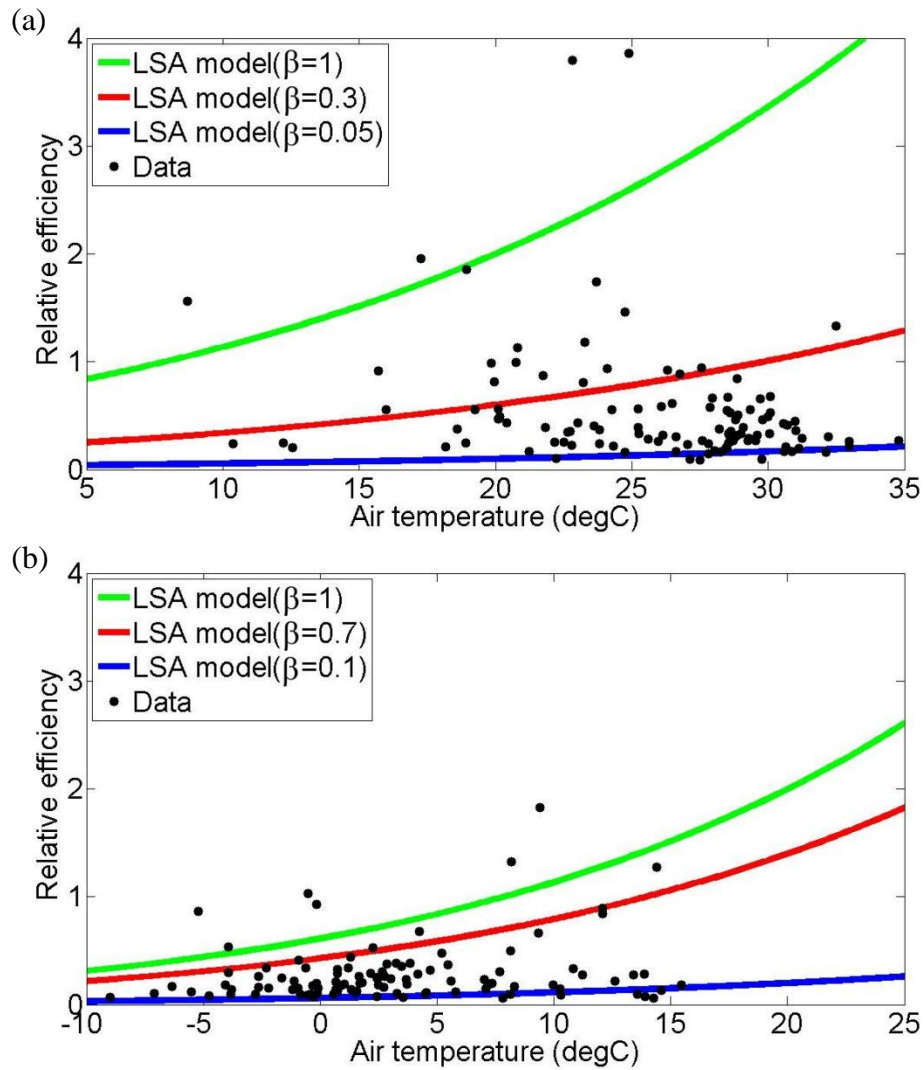
Figure 5.4. Relative efficiency of LE over suburban area from LSA model: (a)

summer (b) winter

Results from the MEP theory and classical method are shown in Figure

5.5. Priestley model is overestimating the relative efficiency of *LE*. Data fit in the

MEP model prediction with β ranging from 0.05 to 0.3 in summer and 0.1 to 0.7

in winter. β ranges are found to be exactly the same as in the LSA model.

Because of the higher surface water availability, relative efficiency in winter is

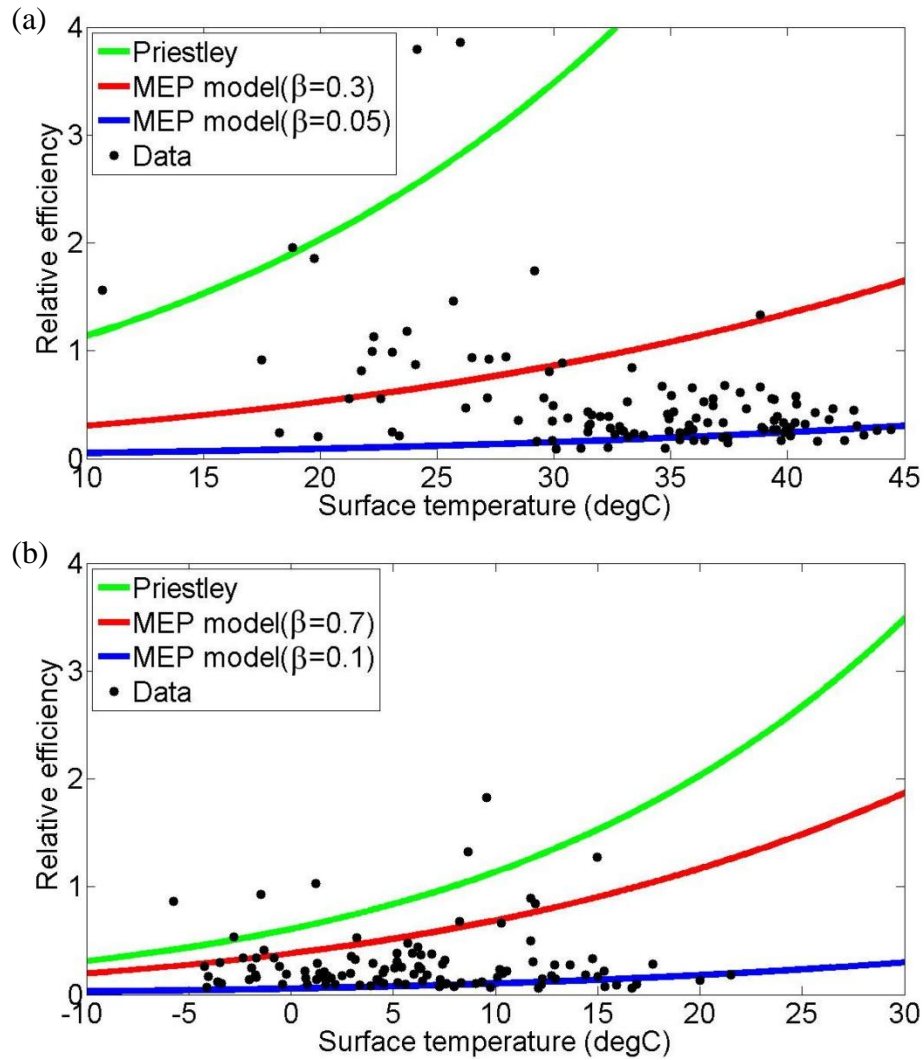shown to be higher than in summer at the same temperature.

Figure 5.5. Relative efficiency of LE over suburban area from MEP theory and Priestley model: (a) summer (b) winter

This phenomenon is largely due to the melting of snow cover in winter time, which is relatively slow and maintains the saturation of surface for a relatively long time as compared to rain precipitation in summer time. In addition, snow over in winter will decrease the temperature difference between the surface and overlying air layer, which leads to a smaller sensible heat flux and eventually a larger relative efficiency of latent heat flux. The difference between the surface

and overlying air layer over suburban surface is shown in Figure 5.6, which is

about 10℃ in summer and 2℃ in winter.
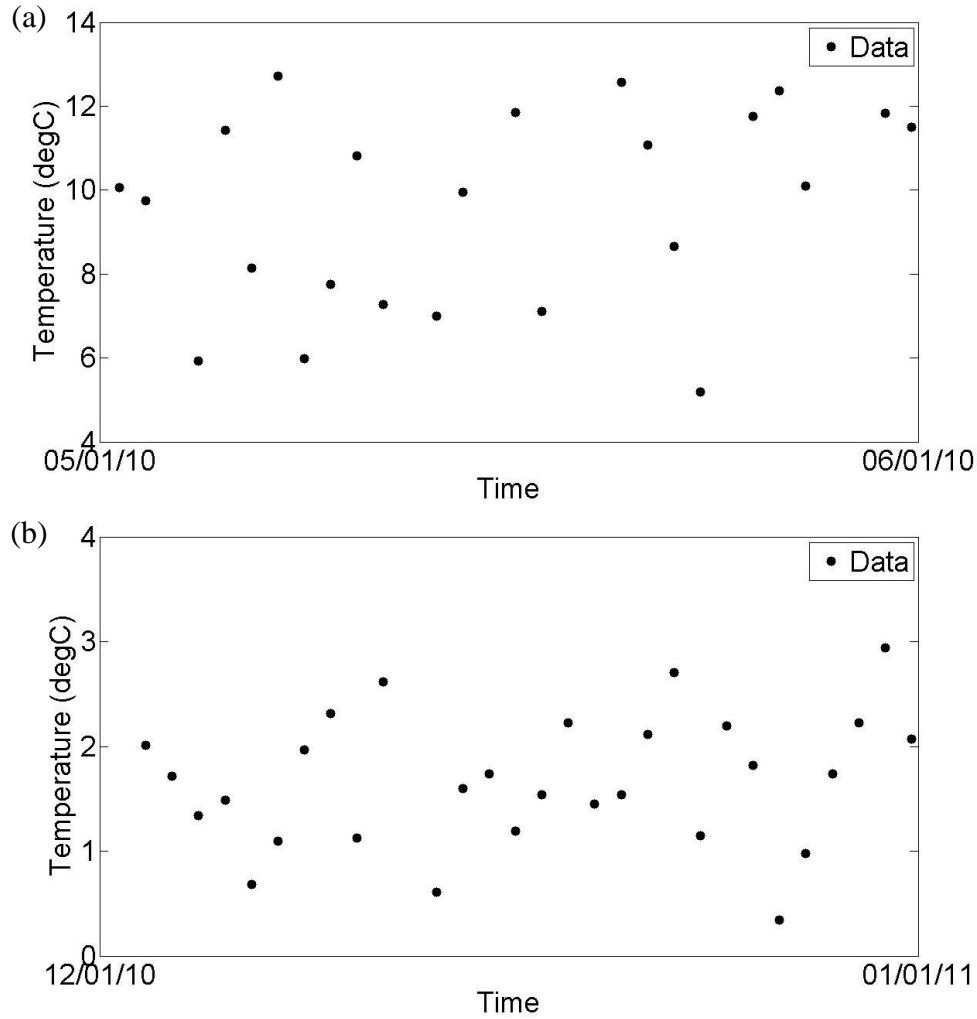
Figure 5.6. Temperature difference between surface and overlying air layer over

suburban area: (a) May 2010 (b) December 2010

Figure 5.7 is showing the relative efficiency of latent heat flux over the

lake surface. As shown in the graphs, all data fit in the result of the LSA model

with β ranging from 0.1 to 0.5. Since the field measurement over the lake

surface is within two months, this result is consistent with the finding over

51

suburban surface. Besides, trends at four different measurement heights are almost identical from the data. This can lead to the conclusion that the height is not playing an important role in affecting the relative efficiency within the measurement range. Over lake, the surface is with full water availability that β is expected to be 1. However, the resulted β range is much smaller. Latent heat has a linear relationship with the evaporation rate which is determined by the difference in saturated vapor pressure between surface and overlying air layer. Based on this, this result indicates that the difference is not as large as expected. In other words, air layer over the lake surface within the measurement range has high humidity that is close to saturated conditions.

In figure 5.8, results from the MEP theory show the same range of β as in the LSA model. The difference is that the same value is found with a larger temperature in the MEP model, which makes sense since in convective condition surface temperature is always higher than the air temperature. Priestley model overestimates the relative efficiency significantly.

For grassland data, field measurements are plotted at a monthly scale (see Figure 5.9). In September 2010, data fit in model prediction with β ranging from 0.2 to 0.5. However, for the other three months, data fall in the range with $\beta > 1$, with some extreme large values about 8. Obviously relative efficiency of latent heat is underestimated in the LSA model over vegetation surface. With $\beta = 1$, the model is computing the potential evaporation which is the maximum possible evaporation rate over a fully saturated surface. However, the model result is still much smaller than field measurements.
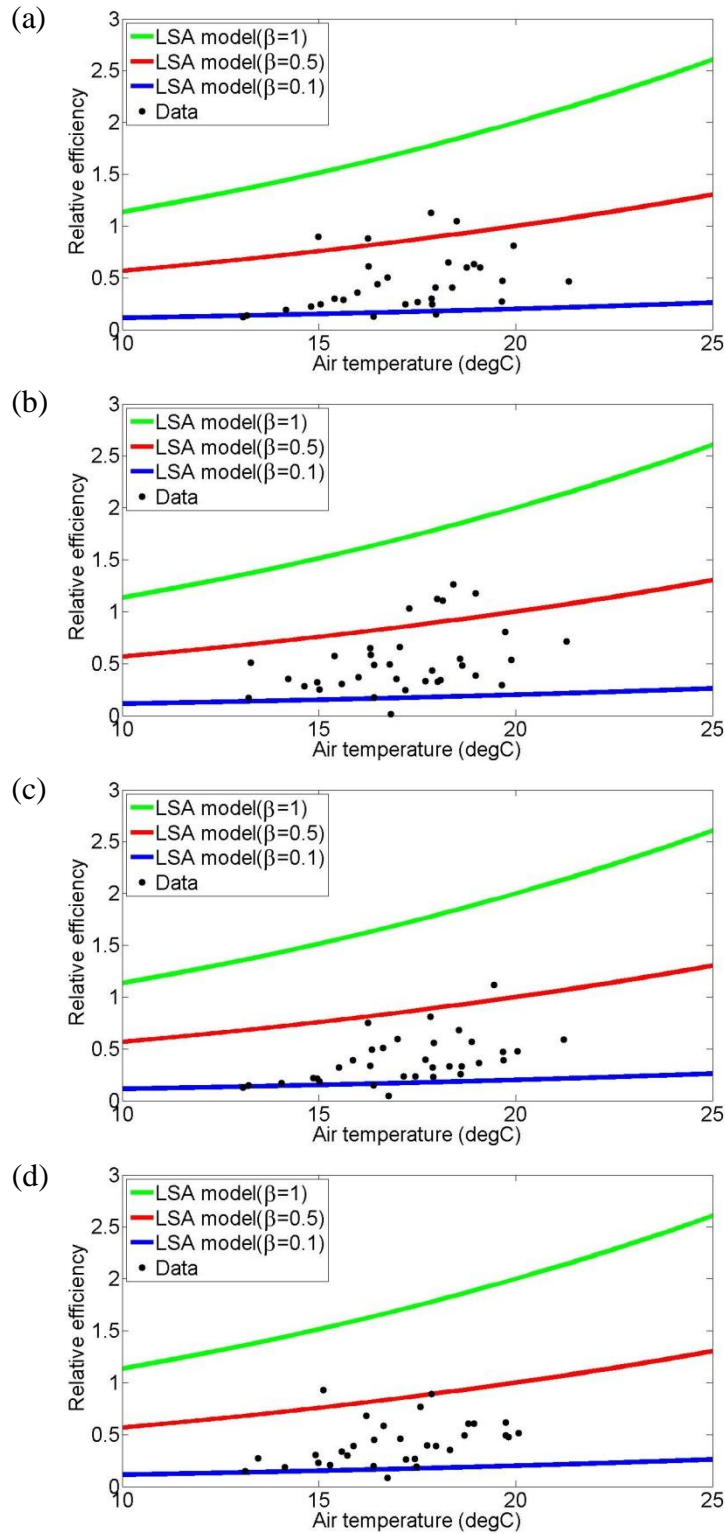
Figure 5.7. Relative efficiency of LE over lake from LSA model: (a) H=1.66m (b)

H=2.31m (c) H=2.96m (d) H=3.61m
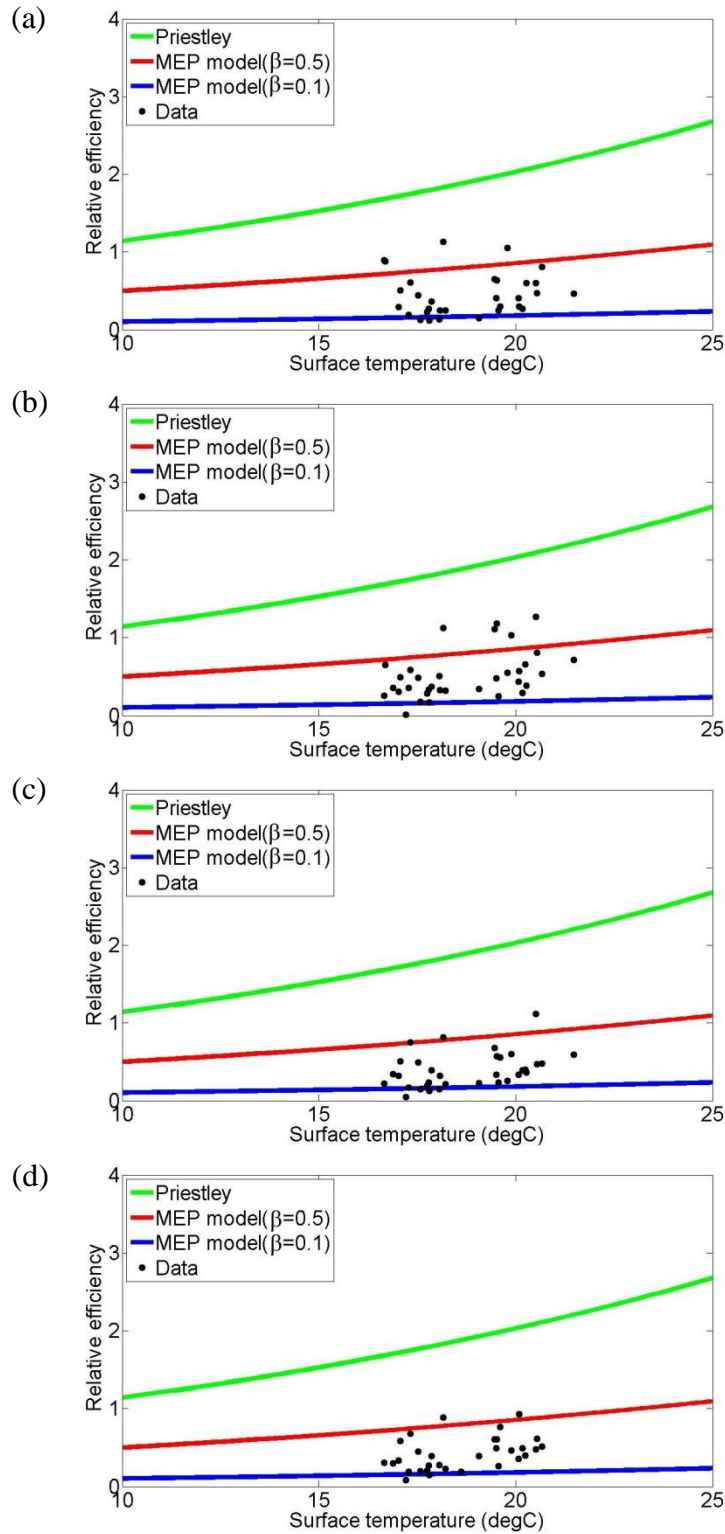
Figure 5.8. Relative efficiency of LE over lake from MEP theory and Priestley

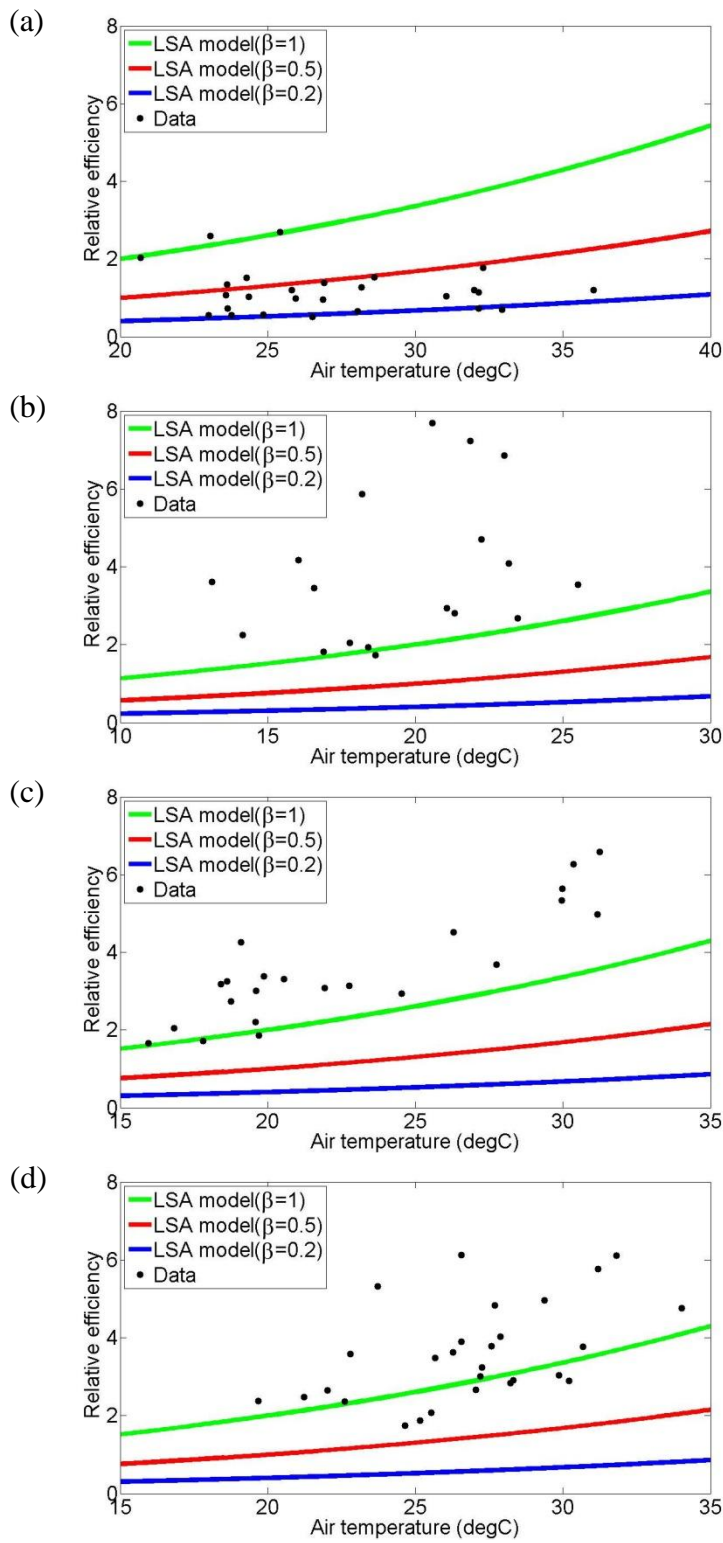model: (a) H=1.66m (b) H=2.31m (c) H=2.96m (d) H=3.61m

Figure 5.9. Relative efficiency of LE over grassland from LSA model: (a)

September 2010 (b) October 2010 (c) May 2011 (d) June 2011

There are different approaches to estimate the potential evaporation rate, but their results are within a small range. Thus, the observed significant deviation is resulted rather from the missing of an important process that contributes to the latent heat flux than from the using of inappropriate equation for evaporation. Over vegetation surfaces, transpiration from plants is found by many researchers, to be significant especially under dense vegetation condition. Among the LSA model, transpiration is not taken into consideration thus the relative efficiency is significantly underestimated.

As introduced in the methodology section, the MEP model over vegetation surfaces will take transpiration into consideration by replacing the surface temperature with the leaf temperature. Unfortunately, leaf temperature was not measured over grassland site. Though not available from field measurements, leaf temperature can be obtained based on its relation with air temperature. Under strong sun exposure condition around noon for thin leaf plants, the difference between air temperature and leaf temperature at maximum will be about $10℃$ (Noffsinger 1961; Linacre 1963). In this study, $5℃$ is adopted as the difference between air temperature and leaf temperature to illustrate the performance of the MEP model over vegetation surface. Results are shown in figure 5.10.
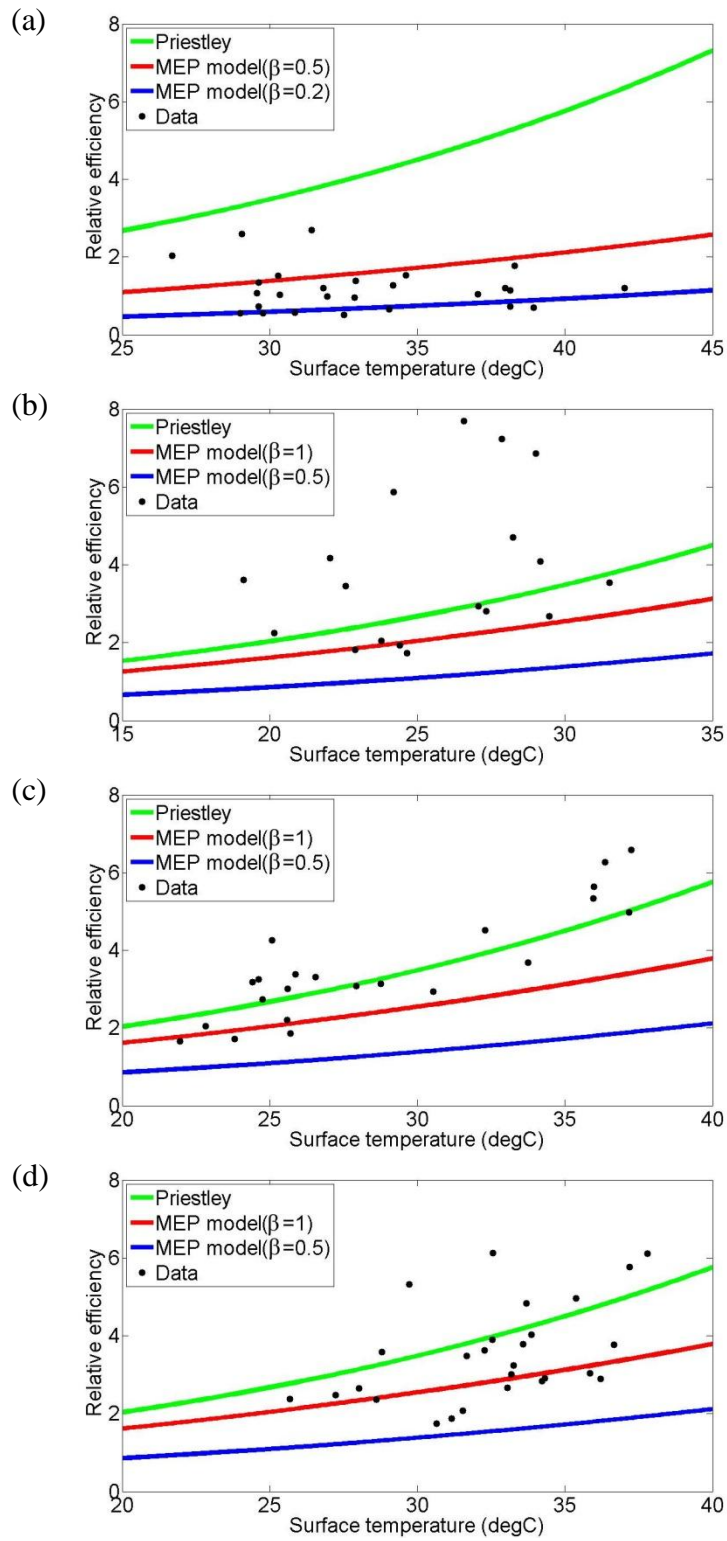
Figure 5.10. Relative efficiency of LE over grassland from MEP theory and

Priestley model: (a) Sep 2010 (b) Oct 2010 (c) May 2011 (d) Jun 2011

Compared to Figure 5.9, Figure 5.10 shows that after taking transpiration into account, the MEP model and Priestley model are having a better prediction than the LSA model over grassland surface. For September and October in 2010, the result is almost the same as from LSA model. However in 2011, good agreement with field measurements is observed in MEP and Priestley model in May and June. MEP and Priestley model basically capture the field observation with the fully saturated condition. The relative efficiency of latent heat increases dramatically from September to October in 2010, which stands for two extreme cases that this period is believed to be the growing season of grasses. Besides, it is important to note that the result here is from the assumptive temperature difference between air layer and leaf surface. Future experiment is encouraged to verify the performance of the MEP and Priestley model over vegetation surface.

5.2.2   Outgoing longwave radiation

As shown in Figure 5.11, relative efficiency of outgoing longwave radiation (OLR) from field measurements is orders of magnitude away from the LSA model prediction over lake surface. Result from the LSA model is around 0.3 while data concentrate in the range from 2 to 8, showing a clear increasing trend with respect to the air temperature. Consistent with the finding in relative efficiency of *LE,* height barely affects the relative efficiency of *OLR* within the measurement range. In the LSA model, relative efficiency of *OLR* is determined by r_a / r_0 . Since r_a is constant in this study, the relative efficiency becomes a reciprocal function of r_0 and is a function of T_a^3. Despite the huge deviation

from model prediction, data are showing a clearly increasing trend with air temperature, which indicates the existence of underlying mathematical description. A linear equation with respect to T_a^3 is used to fit the data: $OLR/H = 1 \times 10^{-6} T_a^3 - 20$. The function shows good agreement with data at different heights within the measurement range.

Same deviation between data and model prediction is observed over suburban surface. However, an interesting phenomenon is found that the relative efficiency is higher in winter than that in summer. This is consistent with the statement that snow cover will decrease the sensible heat over suburban surface in winter. In this case, since outgoing longwave radiation has relatively constant values as a function of T_s^4, reduction in sensible heat will explain the increase in relative efficiency of OLR.

Besides the truncation, other sources may exist causing the deviation between field measurements and model prediction. One possible source will be the use of constant aerodynamic resistance in the study. Precise estimation of aerodynamic resistance is suggested to be included for model improvements.

Another important thing to note here is that the relative efficiency of OLR is higher over lake surfaces than the suburban surface. This can be caused by the oasis effect which reduces the magnitude of sensible heat flux. A linear equation with respect to T_a^3 fitting the suburban data is given in figure 5.12. Remember that the fitting line is only used to illustrate the possibility of mathematical description of the data for future models.
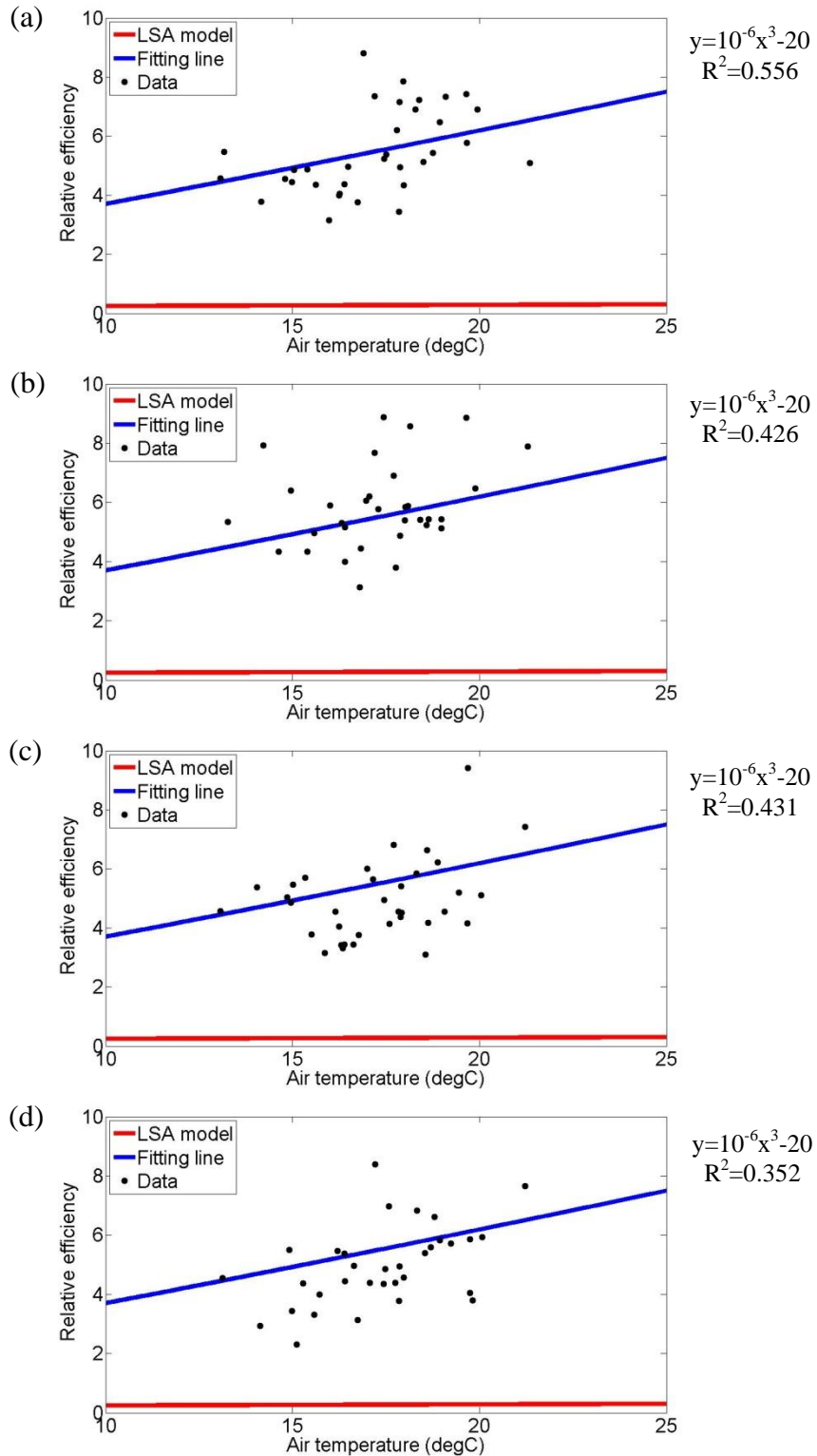
Figure 5.11. Relative efficiency of OLR over lake from LSA model: (a) H=1.66m

(b) H=2.31m (c) H=2.96m (d) H=3.61m
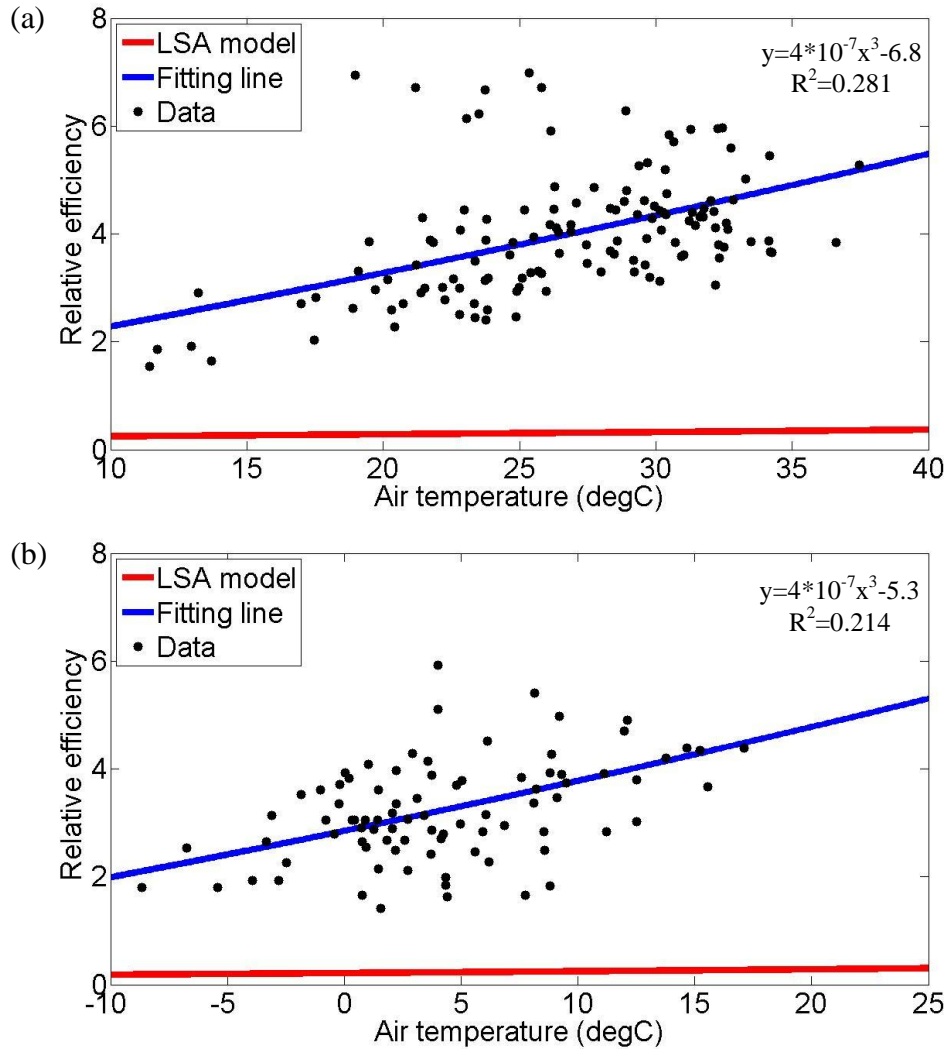
Figure 5.12. Relative efficiency of OLR over suburban area from LSA model: (a) summer (b) winter

5.2.3   Ground heat flux

For ground heat flux, only grassland data is available to verify the model performance. Since sensible heat is included in the mathematical expression, relative efficiency of G in the MEP model is not a continuous function thus the plot of it is separated. It is shown in Figure 5.13 that LSA model and Priestley

model are predicting the relative efficiency of G within a small range around 0.4. This is consistent with the statement concluded from equation (2.3) and equation (2.27) that the relative efficiency of G is determined by the thermal properties of the contacting media. For September 2010, field measurement is smaller than the model prediction, during which the relative efficiency of LE is much smaller than that of other three months. For other three months, data deviates from the model prediction significantly. However, data are still within a small range from 0.2 to 1.5 that the model captures the scale of the relative efficiency of G.

The resulted relative efficiency of G from MEP theory is a function dependent on β and surface temperature. As shown in Figure 2.5, the relative efficiency is insensitive to the surface temperature. Based on this conclusion, the result can be plotted with respect to air temperature since surface temperature is not available. In figure 5.14, it is shown that the results from MEP model are within a small range around 0.4, insensitive to β values. This result is similar to those from the LSA model and Priestley model, which further proves that the thermal properties of the contacting media are determining variables for the relative efficiency of G. One reason for the deviation between the model prediction and field measurements is that measurements of diurnal variations are non-equilibrium while the MEP theory is based on thermodynamic laws of equilibrium state. The deviation may also be caused by using the isotropic and homogeneous thermal property for soils, while vegetated land cover does not possess ideal soil formation due to the root zones.
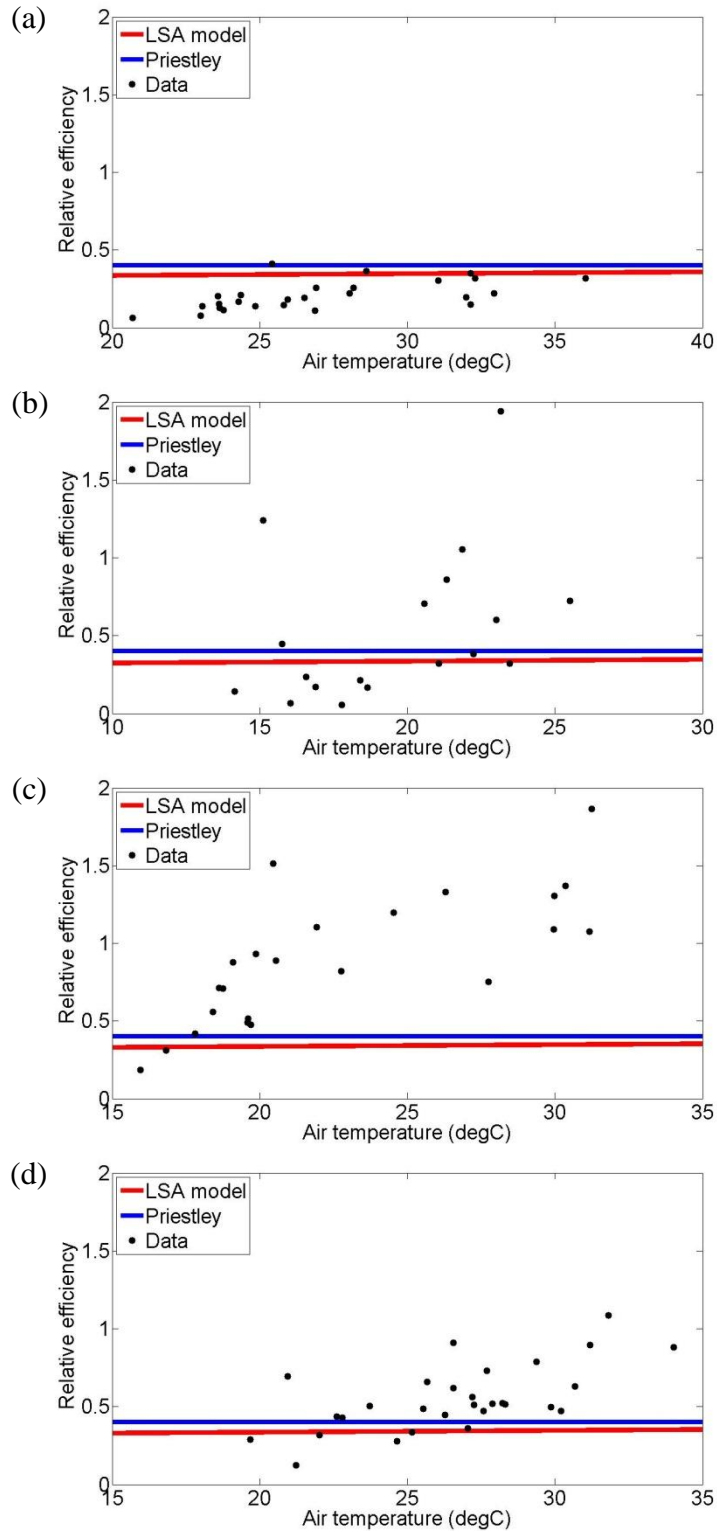
Figure 5.13. Relative efficiency of G over grassland from LSA and Priestley

model: (a) Sep 2010 (b) Oct 2010 (c) May 2011 (d) Jun 2011
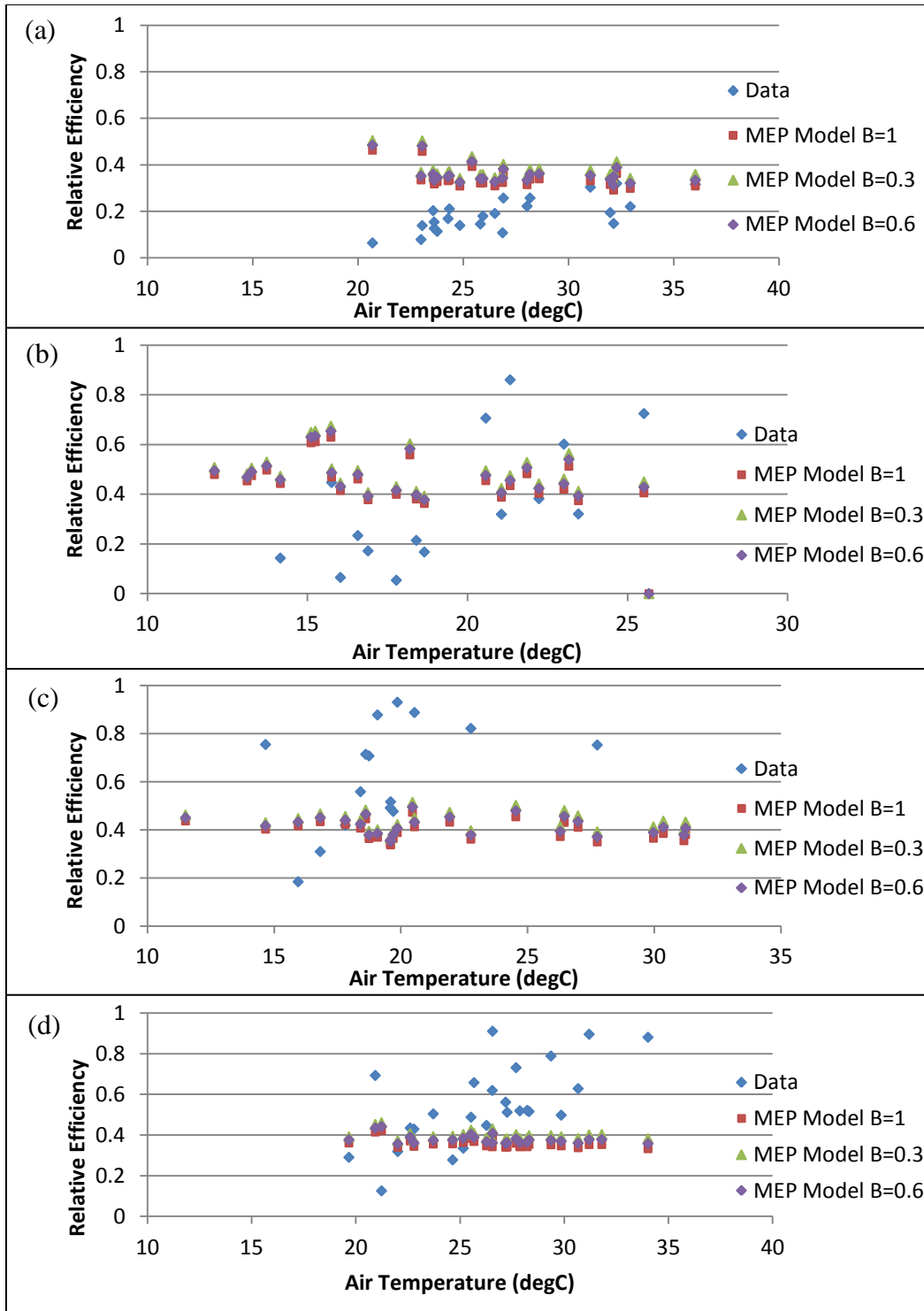
Figure 5.15. Relative efficiency of G over grassland from MEP theory: (a) Sep

2010 (b) Oct 2010 (c) May 2011 (d) Jun 2011

Besides, an increasing trend with respect to temperature is shown clearly by data but not captured by the models. Note that relative efficiency of LE is also increasing with temperature. It indicates that evaporation rate is larger at a higher leaf temperature. In order to support this higher evaporation, roots are taking water from underground aquifers. This root uptake process will increase the heat capacity of soil and eventually increase the relative efficiency of G. Thus the relative efficiency of G is increasing with temperature. In addition, aspiration and photosynthesis of plants can affect the evaporation rate over the vegetation surface. In future models, these biological processes of plants are suggested to be considered over vegetation surface.

Chapter 6

SUMMARY AND FUTURE WORK

6.1 Summary

        The relations between dissipative fluxes in the surface energy budget can

be expressed in terms of the relative efficiency. This relative efficiency is found to

be different over various land covers. Three models of relative efficiency with

good performance are intercompared and verified with a variety of field

observations in this study. Several important conclusions are drawn from the

results.

        In order to apply the theoretic models of relative efficiency to land

surfaces with limited soil moisture availability, water availability parameter β is

introduced by Bateni and Entekhabi (2012). This parameter is incorporated into

the MEP theory in this study to enable model's application over surface with

limited water availability. Results show that β is a useful parameter to predict

the relative efficiency of latent heat flux under convective condition on a daily

scale. Though the value is changing on a daily basis depending on weather

conditions, it concentrates in a certain range that represents the seasonal surface

moisture condition at the experiment site. The introduction of the water

availability parameter enables models to predict temporal variations of the

evaporation efficiency, over a wider range of land cover types.

        In this study, it is found that relative efficiency of latent heat from the

MEP theory is almost identical to that from the LSA model. Over lake and

66

suburban surfaces, both models predict the relative efficiency with the same β

values. Note that the LSA model is dependent on air temperature and MEP theory

is determined by surface temperature. Models can be selected based on the

availability of temperature measurements. For Priestley model, it only predicts

results over saturated surface thus is overestimating the relative efficiency of

latent heat flux over suburban and lake surface where the surface water

availability is found to be smaller than 1.

　　　With only evaporation taken into consideration, LSA model does not have

good performance over vegetation surface, underestimating the relative efficiency

of latent heat flux significantly. The transpiration model is built through replacing

the actual surface by leaf surface. An illustration test proves that this model result

has better agreement with observation over vegetation surface than evaporation

models. Based on the comparison, it is concluded that only evaporation is not

sufficient to predict the latent heat fluxes over vegetation surface, transpiration

should be included in future models.

　　　Over lake surface, the relative efficiency of latent heat is not as high as

commonly expected. One possible reason is that the overlying air layer is almost

saturated near the surface that evaporation is reduced. Another possible reason is

the existence of the oasis effect. The influence of the oasis effect on the relative

efficiencies is unclear and it needs future investigation. Mixing condition is not

changing much within the near surface layer that the height is not playing a

crucial role in the results of relative efficiency within the measurement range. It

should be noted that the real vertical profile of water vapor flux is usually very

complex. Therefore the conclusion is only drawn within the measurement range of the experiment, which is from 1.66 m to 3.61 m above the lake surface.

Separating and treating the surface temperature and air temperature as two systems is reasonable, as supported by the field observation. However, the linearization of surface temperature around air temperature using truncated Taylor's series leads to discrepancies, particularly for processes having nonlinear dependence on temperatures. Significant deviation is observed between the data and model prediction of relative efficiency of outgoing longwave radiation, due to the linearization of the fourth-power (highly nonlinear) law of thermal radiation and the use of constant aerodynamic resistance. However, the fitting line suggests that a mathematical description is possible to describe the relative efficiency through the linearization of surface temperature around air temperature.

For ground heat flux, all models predict similar results, capturing the magnitude of the relative efficiency but with a relatively large deviation. Indicated from model results, the relative efficiency of ground heat flux are determined by the thermal properties of the contacting media to a great extent, insensitive to both the soil water availability and surface temperature. A rapid increasing trend shown by the data with respect to temperature indicates that the change of soil thermal properties caused by the biological processes of plants, especially the root water uptake process, should be considered in future models over vegetation surface.

6.2   Future work

In this study, relative efficiency of outgoing longwave radiation was predicted by the LSA model. However, the result is orders of magnitude from the field measurements. Since longwave radiation can be estimated by a single variable function of surface temperature, it can be obtained at a large scale based on the remote sensed temperature data. Knowing the relative efficiency of the radiation, the estimation of all turbulent fluxes can be achieved at the scale where remote sensing data is available. Thus the relative efficiency of outgoing longwave radiation is of great importance. Deriving the relative efficiency of outgoing longwave radiation by using different numerical linearization approaches in LSA model or by introducing it into MEP theory is the first future work. As suggested by this study, estimation of aerodynamic resistance will be taken into consideration. Comparison of the new result to the field measurement will give suggestions for further steps.

One motivation of this study is to develop mitigation strategies for the urban heat island effect. Current experiment setups on the site will be extended for enabling the estimation of turbulent fluxes. Once the fluxes over different commonly used urban pavements are obtained, relative efficiency of them can be derived and compared to model predictions. And this work can be extended to purely impervious built environment made of engineering materials. The resulted relative efficiency of fluxes can be incorporated into urban canopy models, comparison will be carried out to test if the relative efficiency improves the model performances by specifying the energy partitioning processes over surface of

different materials. Practical application will be to provide realistic strategies in urban planning and design for more sustainable cities.

In this study, models were developed based on the surface energy balance. Field measurements of the surface energy budgets indicate that the energy balance is rarely, if not impossible, observed at timescales less than several hours. And the effect of imbalance to energy partitioning process is unknown. In order to predict the more practical energy partitioning process, the residual of the surface energy budget will be incorporated into models for future theoretic development. After introducing the residual as another term into the surface energy budget, relative efficiency will be rederived from the models. This work will help to find out the mechanism of energy storage over different land covers and the effect of it to the relative efficiency of dissipative fluxes.

Another future work will be applying the relative efficiency in this study at a global scale to observe the long term effect of climate change. The continuous emission of greenhouse gases, aerosols, chloro flouro carbons by human activities has already affected and will keep affecting the radiative forcing conditions of the Earth. The climate responses to the change in radiative forcing conditions have been examined by researchers and the increase in air temperature is commonly predicted (Hansen et al. 1997; Knutti and Hegerl 2008; Schmittner et al. 2011).
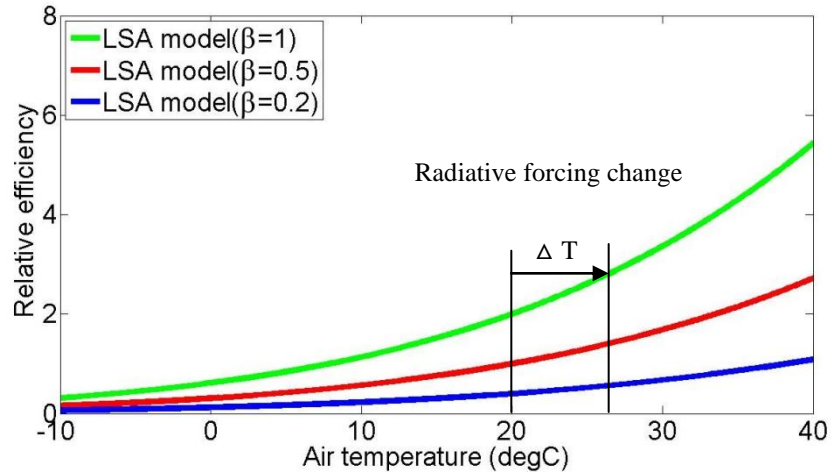
Figure 6.1. Schematic of increase in relative efficiency.

To observe the effect of climate change on relative efficiency, the first
step will be to obtain the increase in temperature from a reliable prediction. Then
based on the temperature difference, increase in relative efficiency of latent heat
can be computed (see Figure 6.1). The increase is determined by the surface water
availability, land cover types and the initial temperature. The final step is to
divide the global area into blocks based on the land cover types and compute the
increase in relative efficiency for each block. At last the long term effect of
climate change caused by different radiative forcing on the global relative
efficiency of latent heat flux can be obtained.

REFERENCES

Anderson, M. C., J. M. Norman, G. R. Diak, W. P. Kustas, and J. R. Mecikalski. 1997. A two-source time-integrated model for estimating surface fluxes using thermal infrared remote sensing. *Remote Sens. Environ.*, 60(2): 195–216.

Arya, S. P. 1988. *Introduction to Micrometeorology*. New York: Academic Press.

Bateni, S. M. and D. Entekhabi. 2012. Relative efficiency of land surface energy balance components. *Water Resour. Res.*, 48: W04510.

Bowen, I. S. 1926. The ratio of heat losses by conduction and by evaporation from any water surface. *Physical Review*, 27: 779–787.

Businger, J. A., J. C. Wyngaard, Y. Izumi, and E. F. Bradle. 1971. Flux-Profile Relationships in the atmospheric surface layer. *J. Atmos. Sci.*, 28: 181– 189.

Cramer, Harrison E. and Frank A. Record. 1953. The variation with height of the vertical flux of heat and momentum. *Jour.Meteorol.*, 10(3): 219-226.

Crow, W. T. and W. P. Kustas. 2005. Utility of assimilating surface radiometric temperature observations for evaporative fraction and heat transfer coefficient retrieval. *Boundary Layer Meteorol.*, 115(1): 105–130.

Deacon, E. L. 1955. *The turbulent transfer of momentum in the lowest layers of the atmosphere.* Melbourne: Commonwealth Scientific and Industrial Research Organization.

Deacon, E. L. and Swinbank, W. C. 1956. Comparison between momentum and water vapor transfer. *Climatology and Microclimatology. Proc. Canberra Symp. UNESCO Arid Zone Res.*, 11: 38-41.

Dewar, R. C. 2003. Information theory explanation of the fluctuation theorem, maximum entropy production and self-organized criticality in non-equilibrium stationary states. *J. Phys. A Math. Gen.*, 36: 631– 641.

Dewar, R. C. 2005. Maximum entropy production and the fluctuation theorem. *J. Phys. A Math. Gen.*, 38: L371–L381.

Dickinson, R. E. 1988. The force-restore model for surface temperatures and its generalizations. *J. Clim.*, 1(11): 1086–1098.

Gentine, P., D. Entekhabi, A. Chehbouni, G. Boulet, and B. Duchemin. 2007. Analysis of evaporative fraction diurnal behavior. *Agric. For. Meteorol.*, 143(1–2): 13–29.

Gentine, P., J. Polcher and D. Entekhabi. 2011. The diurnal behavior of evaporative fraction in the soil-vegetation-atmospheric boundary later continuum. *J. Hydrometeorol.*, 12: 1530–1546.

Hansen, J., M. Sato and R. Ruedy. 1997. Radiative forcing and climate response. *J. Geophys. Res.*, 102: 6831-6864.

Jaynes, E. T. 1957. Information theory and statistical mechanics. *Phys. Rev.*, 106: 620–630.

Jiang, L. and S. Islam. 2001. Estimation of surface evaporation map over Southern Great Plains using remote sensing data. *Water Resour. Res.,* 37(2): 329–340.

Kaimal, J. C. and D. A. Haugen. 1969. Some errors in the measurement of reynolds stress. *J. App. Meteorol.,* 8: 460–462.

Kalma, J. D., T. R. McVicar, and M. F. McCabe. 2008. Estimating land surface evaporation: A review of methods using remotely sensed surface temperature data. *Surv. Geophys.,* 29: 421–469.

Knutti Reto and Hegerl Gabriele C. 2008. The equilibrium sensitivity of the Earth's temperature to radiation changes. *Nature Geoscience.,* 1(11): 735–743.

Linacre, E. T. 1964. A note on a feature of leaf and air temperatures. *Agricultural Meteorology*, 1(1): 66-72.

Lorenz, E. N. 1960. Generation of available potential energy and the intensity of the general circulation, in *Dynamics of Climate* (R. L. Pfeffer Ed.). Oxford: Pergamon Press.

McMillen, R. T. 1988. An eddy correlation technique with extended applicability to non-simple terrain. *Boundary-Layer Meteorol.,* 43: 231–245.

Mecikalski, J. R. 1999. Estimating fluxes on continental scales using remotely sensed data in an atmospheric-land exchange model. *J. Appl. Meteorol.*, 38(9): 1352–1369.

Minobe, S., Y. Kanamoto, N. Okada, H. Ozawa, and M. Ikeda. 2000. Plume structures in deep convection of rotating fluid. *Nagare*, 19: 395–396.

Mobbs, S. D. 1982. Extremal principles for global climate models. *Q. J. R Meteorol. Soc.*, 108: 535–550.

Moran, M. S., W. P. Kustas, A. Vidal, D. I. Stannard, J. H. Blanford, and W. D. Nichols. 1994. Use of ground-based remotely sensed data for surface energy balance evaluation of a semiarid rangeland. *Water Resour. Res.*, 30: 1339–1349.

Noffsinger, T. L. 1961. Leaf and air temperatures under Hawaii conditions. *Pacific Sci.*, 15: 304-306.

Ozawa, H. and A. Ohmura. 1997. Thermodynamics of a global mean state of the atmosphere—A state of maximum entropy increase. *J. Clim.*, 10: 441–445.

Paltridge, G. W. 1975. Global dynamics and climate—A system of minimum entropy exchange. *Q. J. R. Meteorol. Soc.*, 101: 475–484.

Pasquill, F. 1949. Eddy diffusion of water vapor and heat near the ground. *Proc.Roy.Soc.London*, A, 198: 116-140.

Pond, S. 1968. Some effects of buoy motion on measurements of wind speed and stress. *J.Geophys. Res.,*73: 507–512.

Priestley, C. H. B. 1959. *Turbulent Transfer in the Lower Atmosphere*. Chicago: Univ. of Chicago Press.

Pujol, T. and J. E. Llebot. 1999. Extremal principle of entropy production in the climate system. *Q. J. R. Meteorol. Soc.*, 125: 79–90.

Sandholt, I., K. Rasmussen and J. Andersen. 2002. A simple interpretation of the surface temperature/vegetation index space for assessment of surface moisture status. *Remote Sens. Environ.*, 79: 213–224.

Schmittner, A., Urban, N. M., Shakun, J. D., Mahowald, N. M., Clark, P. U., Bartlein, P. J., Mix, A.C. and Rosell-Melé, A. 2011. Climate sensitivity estimated from temperature reconstructions of the last glacial maximum. *Science,* 334 (6061): 1385–8.

Shannon, C. E. 1948. A mathematical theory of communication. *Bell Syst. Tech. J.*, 27: 379– 423.

Shimokawa, S. and H. Ozawa. 2002. On the thermodynamics of the oceanic general circulation: Irreversible transition to a state with higher rate of entropy production. *Q. J. R. Meteorol. Soc.*, 128: 2115–2128.

Sini, F., G. Boni, F. Caparrini, and D. Entekhabi. 2008. Estimation of large-scale evaporation fields based on assimilation of remotely sensed land temperature. *Water Resour. Res.*, 44: W06410.

Stull, R.B. 1988. *An introduction to boundary layer meteorology*. Dordrecht: Kulwer Academic.

Swinbank, W. C. 1955. An experimental study of eddy transports in the lower atmosphere, in *Division of Meteorological Physics.* Melbourne: Commonwealth Scientific and Industrial Research Organization.

Tanner, C. B. and G. W. Thurtell. 1969. *Anemoclinometer measurements of reynolds stress and heat transport in the atmospheric surface layer*. University of Wisconsin Tech. Rep.

Thornthwaite, C. W. and Holzman, B. 1939. The determination of evaporation from land and water surfaces. *Monthly Weather Rev.*, 67: 4-11.

Vercauteren, N., E. Bou-Zeid, M. B. Parlange, U. Lemmin, H. Huwald, J. S. Selker, and C. Meneveau. 2008. Subgrid-scale dynamics of water vapour, heat, and momentum over a lake. *Boundary-Layer Meteorol.*, 128(2): 205–228.

Vercauteren, N., H. Huwald, E. Bou-Zeid, J. S. Selker, U. Lemmin, M. B. Parlange, and I. Lunati. 2011. Evolution of superficial lake water temperature profile under diurnal radiative forcing. *Water Resour. Res.*, 47: W09522.

Wang, J. and R. L. Bras. 1999. Ground heat flux estimated from surface soil temperature. *J. Hydrol.*, 216: 214– 226.

Wang, J., G. D. Salvucci, and R. L. Bras. 2004. An extremum principle of evaporation. *Water Resour. Res.*, 40: W09303.

Wang, J. and R. L. Bras. 2009. A model of surface heat fluxes based on the theory of maximum entropy production. *Water Resour. Res.*, 45: W11422.

Wang, J., R. L. Bras, G. Sivandran and R. G. Knox. 2010. A simple method for the estimation of thermal inertia. *Geophys. Res. Lett.*, 37: L05404.

Wang, J. and R. L. Bras. 2011. A model of evapotranspiration based on the theory of maximum entropy production. *Water Resour. Res.*, 47: W03521.

Wang Z. H., E. Bou-Zeid and J. A. Smith. 2011. A spatially-analytical scheme for surface temperatures and conductive heat fluxes in urban canopy models. *Boundary-Layer Meteorology*, 138(2): 171-193.

Wang Z. H. and Bou-Zeid E. 2012. A novel approach for the estimation of soil ground heat flux. *Agricultural and Forest Meteorology*, 154-155: 214-221.

Webb, E. K. and Pearman, G. I. 1977. Correction of CO2 transfer for the effect of water vapor transfer, in *Second Australasian Conference on Heat and Mass Transfer* (R. W. Bilger Ed.). Sydney: University of Sydney.

Webb, E. K., Pearman, G. I., and Leuning, R. 1980. Correction of flux measurements for density effects due to heat and water vapor transfer. *Quart. J. Roy. Meteorol. Soc.,* 106: 85–100.

Wilczak, J. M., S. P. Oncley, and S. T. Stage. 2001. Sonic Anemometer tilt correction algorithms. *Boundary-layer Meteorology*, 99: 127-150.